AD-A141 788 APPLICATIONS OF THE SCANNING ELECTRON MICROSCOPE TO CONCRETE FAILURE (AXI..(U) STEVENS INST OF TECH HOBOKEN N J K DERUCHER 05 MAR 84 AFOSR-TR-84-0431 1/2

UNCLASSIFIED AFOSR-80-0256 F/G 11/2 NL

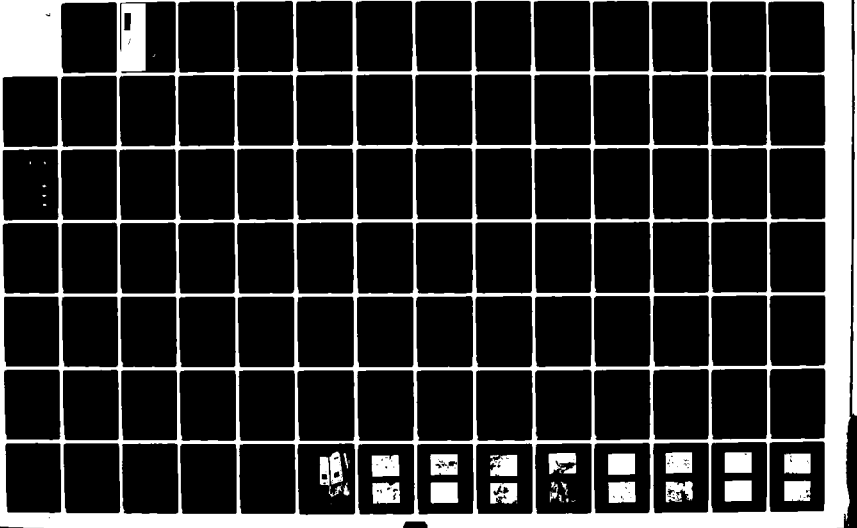

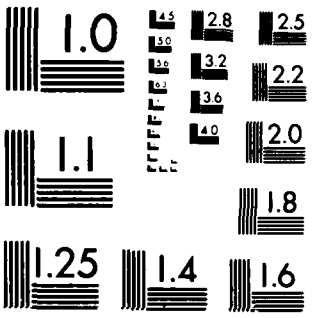

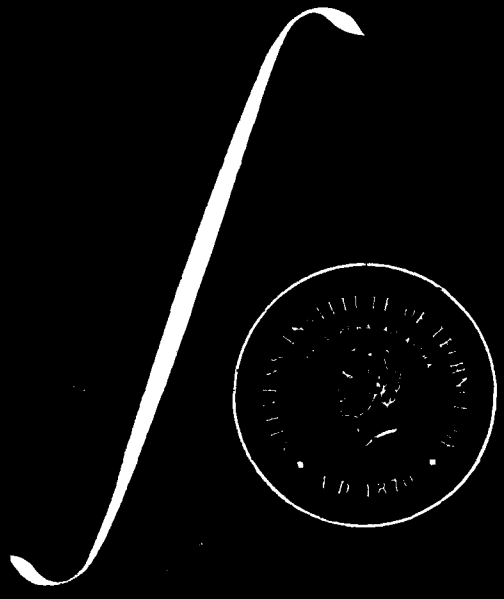

STEVENS INSTITUTE OF TECHNOLOGY

CASTLE POINT STATION

HOBOKEN, NEW JERSEY 07030

APPLICATIONS OF THE SCANNING ELECTRON MICROSCOPE TO CONCRETE FAILURE (Axial, Biaxial, and Dynamic)

AIR FORCE OFFICE OF
SCIENTIFIC RESEARCH
BOLLING AFB, D.C. 20332

STEVENS INSTITUTE OF TECHNOLOGY
DEPARTMENT OF CIVIL AND OCEAN ENGINEERING
HOBOKEN, NEW JERSEY 07030

PERFORMANCE: 1980-1983

AFOSR-80-0256
FINAL

"Qualified requestors may obtain additional copies from the Defense Technical Information Service."

CONDITIONS OF REPRODUCTION

SECURITY CLASSIFICATION OF THIS PAGE *(When Data Entered)*

REPORT DOCUMENTATION PAGE		READ INSTRUCTIONS BEFORE COMPLETING FORM
1. REPORT NUMBER AFOSR-TR- 84-0431	2. GOVT ACCESSION NO. AD-A141785	3. RECIPIENT'S CATALOG NUMBER
4. TITLE *(and Subtitle)* Applications of the Scanning Electron Microscope to Concrete Failure		5. TYPE OF REPORT & PERIOD COVERED FINAL 1 Sep. 80 - 31 Aug. 83
		6. PERFORMING ORG. REPORT NUMBER
7. AUTHOR(s) K. Derucher		8. CONTRACT OR GRANT NUMBER(s) AFOSR-80-0256
9. PERFORMING ORGANIZATION NAME AND ADDRESS Stevens Institute of Technology Department of Civil Engineering Hoboken, New Jersey 07030		10. PROGRAM ELEMENT, PROJECT, TASK AREA & WORK UNIT NUMBERS 61102F 2307/C2
11. CONTROLLING OFFICE NAME AND ADDRESS Air Force Office of Scientific Research/NA Bolling AFB, DC 20332		12. REPORT DATE March 5, 1984
		13. NUMBER OF PAGES 94
14. MONITORING AGENCY NAME & ADDRESS *(if different from Controlling Office)*		15. SECURITY CLASS. *(of this report)* Unclassified
		15a. DECLASSIFICATION/DOWNGRADING SCHEDULE

16. DISTRIBUTION STATEMENT *(of this Report)*

Approved for Public Release; Distribution Unlimited

17. DISTRIBUTION STATEMENT *(of the abstract entered in Block 20, if different from Report)*

18. SUPPLEMENTARY NOTES

19. KEY WORDS *(Continue on reverse side if necessary and identify by block number)*

Concrete Failure
Microcracks
Scanning Electron Microscope

20. ABSTRACT *(Continue on reverse side if necessary and identify by block number)*

Many investigators have implied that the failure mechanism of concrete is associated with internal microcracking. The information and propagation of such microcracks have been studied indirectly by sonic velocity, acoustic methods, and by the observation of macrocracks on the surface of the models. Robinson and Hsu, Slate, Sturrman and Winter have directly observed the formation and propagation of microcracks by X-ray analysis. Due to the limitation in the technique employed, the detection of microcracks was somewhat uncertain. Further, Hanson in an attempt to verify the conclusions of Hse et al., disagreed on some aspect

DD FORM 1 JAN 73 1473

Unclassified

SECURITY CLASSIFICATION OF THIS PAGE

of their findings. Thus, it is apparent from the differences in the data received, the techniques employed, and the theories utilized by the various researchers that further basic research was needed in the field of concrete microcracking. A better understanding of the failure mechanism of concrete (at the micro-level) may provide a more knowledgeable understanding of the engineering properties of concrete, possibly leading to developments for improving these properties and subsequently improved use of concrete materials.

Thus, a three year-three phase research project was established in which the major objective was to directly observe the formation and/or propagation of microcracks in concrete (plain and reinforced) both before and after applications of axial, biaxial, and dynamic stress fields. As part of this objective; procedures, techniques, apparatus, and equipment were developed and/or modified for the study of concrete fracture utilizing the Scanning Electron Microscope (SEM). In addition, information regarding microcracks, propagation of these microcracks (concrete failure), aggregate shape, plain and reinforced concrete, the sum effect of various stress fields, and the ultimate strength of concrete was found.

The results of the first year-phase one study has shown that the SEM is an invaluable tool for the investigation of concrete for both plain and reinforced concrete when subjected to various stress fields (0,15,30,45,60 and 75 percent of the ultimate strength of concrete at 2000, 3000, 4000, and 5000 psi) and loading conditions (axial, biaxial, and dynamic). However, Phase I concerned itself mainly with the failure mechanism of general concrete. By the term general concrete, it is meant that concrete made of or consisting of the five basic concrete making materials (portland, cement, water, air, fine aggregate, and course aggregate). The failure mechanism of concrete containing additional additives was not investigated.

The Phase II-year II project was initiated utilizing the results obtained in Phase I to obtain information on the formation and propagation of microcracks in concrete made with a blended cement for both plain and reinforced concrete both before and after applications of axial, biaxial, and dynamic stress fields utilizing the SEM. In each case the blended cement consisted of a 15 percent replacement material. These additives utilized were pozzolan (fly ash), fly ash-lime and fly ash-lime-sulpher.

Again information regarding microcracks, propagation of these microcracks (concrete fracture), aggregate shape, plain and reinforced concrete, the sum effects of various stress fields, and the ultimate strength of concrete was found for concrete containing blended cements. Thus, knowledge of the failure mechanism of concrete (concrete fracture) utilizing blended cements was needed to facilitate their acceptance for use in structural concrete without compromise on quality.

The Phase III-year III recognized that the failure mechanism of concrete is twofold. First, concrete may fail from applied service loads or applied stress fields whether they are axial, biaxial, or dynamic. Second, concrete may fail as a result of volume changes such as the hydration of the cement paste leading to the shrinkage microcracks or to various cycles of wetting and drying or temperature variations (freezing and thawing). Thus, a model previously developed was investigated and the equations developed were found to be appropriate.

APPLICATIONS OF THE SCANNING ELECTRON MICROSCOPE TO CONCRETE FAILURE

(Axial, Biaxial, and Dynamic)

PROJECT SPONSOR: Air Force Office of Scientific Research
Bolling AFB, D.C.

PERFORMING AGENCY: Stevens Institute of Technology
Department of Civil and Ocean Engineering
Hoboken, New Jersey 07030

PERIOD PERFORMANCE: 1980-1983

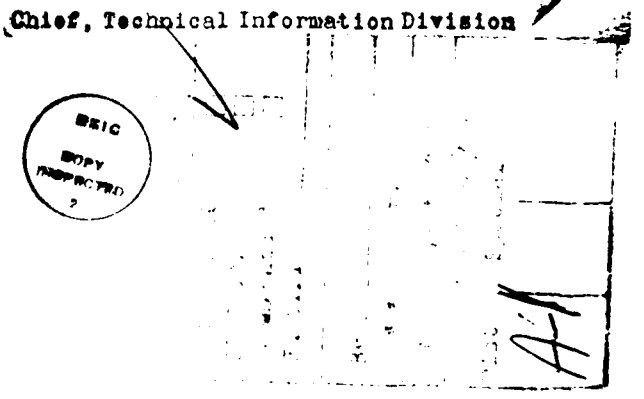

TABLE OF CONTENTS

APPLICATIONS OF THE SCANNING ELECTRON MICROSCOPE TO CONCRETE FAILURE

(Axial, Biaxial, and Dynamic)

ABSTRACT

Many investigators have implied that the failure mechanism of concrete is associated with internal microcracking. The information and propagation of such microcracks have been studied indirectly by sonic velocity, acoustic methods, and by the observation of macrocracks on the surface of the models. Robinson and Hsu, Slate, Sturnman and Winter have directly observed the formation and propagation of microcrakcs by X-ray analysis. Due to the limitation in the technique employed, the detection of microcracks was somewhat uncertain. Further, Hanson, in an attempt to verify the conclusions of Hsu et al., disagreed on some aspect of their findings. Thus, it is apparent from the differences in the data received, the techniques employed, and the theories utilized by the various researchers that further basic research was needed in the field of concrete microcracking. A better understanding of the failure mechanism of concrete (at the micro-level) may provide a more knowledgeable understanding of the engineering properties of concrete, possibly leading to developments for improving these properties and subsequently improved use of concrete materials.

Thus, a three year - three phase research project was established in which the major objective was to directly observe

the formation and/or propagation of microcracks in concrete (plain and reinforced) both before and after applications of axial, biaxial, and dynamic stress fields. As part of this objective; procedures, techniques, apparatus, and equipment were developed and/or modified for the study of concrete fracture utilizing the Scanning Electron Microscope (SEM). In addition, information regarding microcracks, propagation of these microcracks (concrete failure), aggregate shape, plain and reinforced concrete, the sum effect of various stress fields, and the ultimate strength of concrete was found.

The results of the first year - phase one study has shown that the SEM is an invaluable tool for the investigation of concrete for both plain and reinforced concrete when subjected to various stress fields (0, 15, 30, 45, 60 and 75 percent of the ultimate strength of concrete at 2000, 3000, 4000, and 5000 psi) and loading conditions (axial, biaxial, and dynamic). However, Phase I concerned itself mainly with the failure mechanism of general concrete. By the term general concrete, it is meant that concrete made of or consisting of the five basic concrete making materials (portland, cement, water, air, fine aggregate, and course aggregate). The failure mechanism of concrete containing additional additives was not investigated.

The Phase II - year II project was initiated utilizing the results obtained in Phase I to obtain information on the formation and propagation of microcracks in concrete made with a

a blended cement for both plain and reinforced concrete both before and after applications of axial, biaxial, and dynamic stress fields utilizing the SEM. In each case the blended cement consisted of a 15 percent replacement material. These additives utilized were pozzolan (fly ash), fly ash-lime and fly ash-lime-sulpher.

Again information regarding microcracks, propagation of these microcracks (concrete fracture), aggregate shape, plain and reinforced concrete, the sum effects of various stress fields, and the ultimate strength of concrete was found for concrete containing blended cements. Thus, knowledge of the failure mechanism of concrete (concrete fracture) utilizing blended cements was needed to facilitate their acceptance for use in structural concrete without compromise on quality.

The Phase III - year III recognized that the failure mechanism of concrete is twofold. First, concrete may fail from applied service loads or applied stress fields whether they are axial, biaxial, or dynamic. Second, concrete may fail as a result of volume changes such as the hydration of the cement paste leading to the shrinkage microcracks or to various cycles of wetting and drying or temperature variations (freezing and thawing). These areas were investigated in the Phase III - year III project, thus a model previously developed was investigated and the equations developed were found to be appropriate.

INTRODUCTION

Many investigators have implied that the failure mechanism of concrete is associated with internal microcracking (1-6). The formation and propagation of such microcracks in plain and reinforced concrete have been studied indirectly by sonic velocity, acoustic methods, and by the observation of mac· ·racks on the surface of the models, Robinson (7) and Hsu, Slat(Sturman and Hinter (8) have directly observed the format . and propagation of microcracks in plain concrete by X-ray ana _is. Due to the limitations in the technique employed, the detection of microcracks was somewhat uncertain.

In addition, Hsu et al. used a light microscope at 40x magnification to verify the results of X-ray analysis. They examined cross-sections of concrete (0.15 in. thick) both before and after application of axial compressive stress fields. In those concrete models which were examined after application of axial compressive stress fields, the concrete was sliced perpendicular to the direction of the applied load. Prior to slicing and examination of the concrete models, they were subjected to various axial compressive stress fields and the loads were subsequently removed.

According to Hsu et al., three types of microcracks were identified: bond, matrix, and aggregate microcracks. Further, bond microcracks (microcracks between the cement mortar matrix and aggregate particles) exist in the form of shrinkage microcracks prior to application of axial compressive stress fields.

These initial microcrakcs begin to propagate at approximately 30-40% of the ultimate strength. The stress-strain curve deviates from linearity at this point, and there is an increase in the lateral expansion of the concrete. Matrix microcracks (microcracks in the cement mortar matrix) are formed by propagating bond microcracks at about 70-90% of the ultimate strength. Aggregate microcracks occur just before failure.

Hansen (9) in an attempt to verify the conclusions of Hsu et al., disagreed on some aspects of their findings. Hansen also tried to observe microcracks in plain concrete both before and after application of axial compressive stress fields, but the axial compressive stress fields were not removed prior to observation. Hansen applied a purely axial compressive stress field to the concrete models and observed (using a light microscope at 50x magnification) the formation and propagation of surface microcracks. Under a purely axial load, microcracks are believed to originate in the center of the concrete and propagate to the outer surface. Hansen, however, did not find bond microcracks in the form of shrinkage microcracks prior to application of axial compressive stress fields under magnifications as high as 1000x with the light microscope. Hansen discovered that bond microcracks (under a magnification of 50x) occurred at about 45% of the ultimate strength unlike the 30-40% figure found by Hsu et al. He agreed that matrix microcracks occur between 70 and 90% of the ultimate strength, and that aggregate

microcracks occur just before failure.

The differences between the results obtained by these two groups of investigators is easily explained. A light microscope as used by Hsu et al., and Hansen at 40x and 50x magnification respectively has poor depth of field. This feature does not permit the peaks and valleys normally encountered on rough fractured surfaces to be imaged in focus, regardless of the magnification. This poor depth of field made it difficult to distinguish between actual microcracks in the matrix and very porous mortar. At lower axial compressive stress fields; Hsu et al., and Hansen may have mistaken the microcracks to be very porous mortar (since the microcracks were only 3 or 4 μm wide) and only when the microcracks reached a proportional size could a difference be made. This may account in part for the higher values received by Hsu et al., and Hansen in their investigation of matrix microcracks. Even though Hsu et al., utilized the X-ray analysis even this method is considered inconsistent and lacks verification as does the sonic velocity and acoustic methods (in both plain and reinforced concrete).

In addition, Hsu et al., removed the axial compressive stress fields prior to observation of microcracks. Many microcracks which formed may have gone unnoticed, because they may have closed due to relief in stress. Again, this may account for in part the high values received by Hsu et al.

In Hansen's investigation, surface microcracks were observed. Hansen applied a purely axial compressive stress field to the concrete models. Under an axial load microcracks are believed to originate in the center of the concrete models and then propagate to the outer surface. Under this assumption microcracks would not be noticed on the surface of the models until higher axial compressive stress fields were reached. This may account for the differences received by Hsu et al. and Hansen as far as bond microcracks are concerned.

As far as biaxial and dynamically loaded concrete is concerned no one has attempted to observe the formation and/or propagation of microcracks in either case whether plain or reinforced concrete.

The approaches used by Hsu et al. and Hansen in the investigation of the failure mechanism of plain concrere (microcracking) were well received at the time and they did add knowledge to the field of concrete technology. However, it is apparent from the differences in the data received, the techniques employed, and the theories utilized by Hsu et al. and Hansen as well as the results of the preliminary investigation and detailed in this report under Preliminary Investigation that further basic research is needed in the field of concrete microcracking. A better understanding of the failure mechanism of concrete (at the micro-level) may provide a more knowledgeable understanding of the engineering properties of both plain and reinforced concrete, possibly leading to developments for improving these properties and subsequently improved use of concrete

materials for roads, airfields, buildings, and bridges. The further development in the application of fracture mechanics (microcracking) to plain and reinforced concrete would be particularly helpful in interpreting, generalizing and extending research results.

PROPOSED RESEARCH

Based on the differences received by the various researchers and the preliminary investigation as well as the fact that these investigators only examined plain concrete under an axial compressive stress field; it was proposed, to develop procedures and techniques to adequately investigate the field of concrete microcracking; i.e., to directly observe the formation and/or propagation of microcracks in plain and reinforced concrete both before and after the application of axial, biaxial, and dynamic stress fields utilizing the Scanning Electron Microscope (SEM).

Thus, a three year - three phase research project was established in which the major objective was to directly observe the formation and/or propagation of microcracks in concrete (plain and reinforced) both before and after applications of axial, biaxial, and dynamic stress fields. As part of this objective; procedures, techniques, apparatus, and equipment were developed and/or modified for the study of concrete fracture utilizing the Scanning Electron Microscope (SEM). In addition, information regarding microcracks, propagation of these microcracks

(concrete failure), aggregate shape, plain and reinforced concrete, the sum effect of various stress fields, and the ultimate strength of conctete was found.

The results of the first year - phase one study has shown that the SEM is an invaluable tool for the investigation of concrete for both plain and reinforced concrete when subjected to various stress fields (0, 15, 30, 45, 60 and 75 percent of the ultimate strength of concrete at 2000, 3000, 4000, and 5000 psi) and loading conditions (axial, biaxial, and dynamic). However, Phase I concerned itself mainly with the failure mechanism of general concrete. By the term general concrete, it is meant that concrete made of or consisting of the five basic concrete making materials (portland, cement, water, air, fine aggregate, and course aggregate). The failure mechanism of concrete containing additional additives was not investigated.

The Phase II - year II project was initiated utilizing the results obtained in Phase I to obtain information on the formation and propagation of microcracks in concrete made with a blended cement for both plain and reinforced concrete both before and after applications of axial, biaxial, and dynamic stress fields utilizing the SEM. In each case the blended cement consisted of a 15 percent replacement material. These additives utilized were pozzolan (fly ash), fly ash-lime and fly ash-lime-sulpher.

Again information regarding microcracks, propagation of these microcracks (concrete fracture), aggregate shape, plain and

reinforced concrete, the sum effects of various stress fields, and the ultimate strength of concrete was found for concrete containing blended cements. Thus, knowledge of the failure mechanism of concrete (concrete fracture) utilizing blended cements was needed to facilitate their acceptance for use in structural concrete without compromise on quality.

The Phase III - year III recognized that the failure mechanism of concrete is twofold. First, concrete may fail from applied service loads or applied stress fields whether they are axial, biaxial, or dynamic. Second, concrete may fail as a result of volume changes such as the hydration of the cement paste leading to the shrinkage microcracks or to various cycles of wetting and drying or temperature variations (freezing and thawing). These areas were investigated in the Phase III - year III by verifying the mathematics of a previous model.

DESIGN OF EXPERIMENTAL INVESTIGATION

Scanning Electron Microscope:

It was decided to use the scanning electron microscope (SEM) as the viewing apparatus (to directly observe microcracks in concrete) because of its unique capabilities and its distinct advantages over other viewing apparatus such as the light microscope. The depth of field and scanning ability are the two main advantages of the SEM, thus, making the SEM particularly well suited for fractography. Its depth of field is many times greater than that

provided by the light microscope for equivalent magnifications. This feature permits both the peaks and valleys normally encountered on rough fractured surfaces to be imaged in focus, even at relatively high magnifications. In addition, the SEM can scan a one-square inch area, and magnify the same area 100,000 times, and obtain a relatively clear, sharp photograph.

Loading Devices:

The loading devices for the study of concrete under axial and biaxial stress fields were designed to allow for the maximum size specimen possible such that the specimen could still fit into the SEM chamber.

When utilizing the loading devices they were set not to exceed 75 percent of the ultimate strength of concrete. The purpose for setting this limit was that concrete is believed to fail at 85 percent of the ultimate load and our objective was to view the concrete from 0 to 75 percent (just before failure).

Applying the Stress:

Since stress cannot be measured directly, it becomes necessary to express stress in terms of strain. Strain is a quantity that can be measured directly. With the aid of a few engineering mechanics formulas the transition from stress to stain is made quite easily. Once the desired strain is known, it is applied to the specimen and measured through the use of SR-4 strain gages. Four strain gages

were utilized. The gauges were placed on the steel bars rather than the concrete. Steel, a homogeneous material, will exhibit uniform strain throughout. Concrete, a heterogeneous material, will not exhibit uniform strain throughout. The strain in the aggregate may be different than the strain in the matrix or the strain associated with the aggregate-matrix bond. This point is verified by the fact that microcracks first appear at the face of the aggregate-matrix bond. The strain must be increased to create matrix and aggregate cracks. As a result of this, if strain gages were placed on the concrete specimen, uncertainty in the actual strains would result. This would probably lead to erroneous results, therefore it is best to place the SR-4 strain gages on the steel members. The stress in the steel will be used to calculate the stress in the concrete.

Scanning Procedure:

Once a specimen is prepared, it will be placed in the loading apparatus and the desired level of stress will be applied. The stress to be applied will vary from 0 to 75% of the ultimate load. The scanning procedure will be the same in all cases regardless of the stress applied. The manner in which the stress is to be applied will be discussed in the next section. The specimen will then be placed in the SEM chamber and allowed to reach high vacuum. The scanning procedure will now begin.

Since the SEM is only capable of scanning a 1" X 1" area the procedure will be as follows: The area to be scanned will move from left to right drop down one-fifth of an inch and scan from right to left. Again drop down one-fifth of an inch and scan from left to right. The procedure will continue in this manner until the entire area is scanned. Photographs of various microcracks may be taken at various points.

Method of Investigation:

In the investigation of microcrakcs under a compressive stress field using the SEM only one method of operation will be utilized. The specimens will be prepared and loaded to their appropriate stress levels. The specimen will be placed in the SEM chamber under zero load at first. (Prior to this the specimen will be scanned for shrinkage microcracks by use of a light microscope at 40x magnification.) The chamber will be allowed to reach high vacuum and the specimen will be scanned for microcracks (shrinkage). The specimen will then be removed and the specimen re-examined by use of a light microscope at 40x magnification. By comparing the three results it will be shown that the SEM in an attempt to reach high vacuum did not produce or expand, and/or propagate microcracks if they existed.

The same specimen (just scanned) will then be subjected to a compressive stress field of 15% of f_c'. The specimen will then be placed back in the SEM chamber. The chamber will then be allowed

to reach high vacuum and the specimen will be scanned in a fashion previously described under Scanning Procedures. At the end of the scanning period of time, the specimen will be removed and the stress will be increased to 30 percent of f_c'. The procedure used previously will be followed and this procedure maintained until 75 percent of f_c'.

Specimen Preparation:

Rather than list each specimen separately and re-discuss it here, it is easier to discuss them under results.

INVESTIGATION AND RESULTS (PHASE 1 - YEAR 1)

General:

During the first year of this research project entitled "Applications of the Scanning Electron Microscope to Concrete Fracture (Axial, Biaxial, and Synamic Testing)" the major objective was to directly observe the formation and/or propagation of microcracks in concrete (plain and reinforced) both before and after applications of axial, biaxial and dynamic stress fields. As part of this objective; procedures, techniques, apparatus, and equipment were developed and/or modified for the study of concrete fracture utilizing the Scanning Electron Microscope (SEM). In addition, some information regarding microcracks, propagation of these microcracks (concrete fracture), aggregate shape, plain

and reinforced concrete, the sum effects of the various stress fields, and the ultimate strength of concrete was found.

Scanning Electron Microscope:

Results have shown that the SEM at 40,000X magnification is an invaluable tool for the investigation of both plain and reinforced concrete when subjected to various stress fields and loading conditions (axial, biaxial, and dynamic).

Concrete Specimens:

Two, three, four and 5,000 psi concrete was used to form sixteen beams 3 X 3 X 14 inches (eight plain and eight reinforced) for each of the stress field parameters considered in Table 1: Axial Stress Field Parameters; Table 2: Biaxial Stress Field Parameters; and Table 3: Dynamic Stress Field Parameter.

For each stress field case for the eight plain beams, four contained rounded aggregate and four contained angular aggregate. In the eight reinforced beams, for each stress field case, four contained rounded aggregate and four contained angular aggregate. Two specimens were sawed from each beam resulting in a total of 32 specimens for each stress field. Each beam prior to sawing was cured for 28 days at $78^{o} \pm 1^{o}F$ and 98 $\pm$ 2% relative humidity. After the curing process, two specimens were sawed from each beam using a diamond blade saw and shaped. The face of each specimen was polished and squared using a surface grinder.

TABLE 1: AXIAL STRESS FIELD PARAMETERS CONSIDERED

Parameters	Model 1	Model 2
Ultimate Strength	2 to 5 ksi (Increments of 1 ksi)	2 to 5 ksi (Increments of 1 ksi)
Axial Stress Fields	15,30,45,60,75%	15,30,45,60,75%
Coarse Aggregate Shape	Rounded	Angular
Fine Aggregare Shape	Rounded	Angular
Top Size of Coarse Aggregate	1 in.	1 in.
Curing Time, Temperature and Humidity	28 days, 70°F 98 ± 2%	28 days, 70°F 98 ± 2%
Number of Samples	16	16

TABLE 2: BIAXIAL STRESS FIELD PARAMETERS CONSIDERED

Parameters	Model 1	Model 2
Ultimate Strength	2 to 5 ksi (Increments of 1 ksi)	2 to 5 ksi (Increments of 1 ksi)
Stress Field in the X-direction	15,30,45,60,75%	15,30,45,60,75%
Stress Field in the Y-direction	15,30,45,60,75%	15,30,45,60,75%
Coarse Aggregare Shape	Rounded	Angular
Fine Aggregate Shape	Rounded	Angular
Top Size of Coarse Aggregate	1 in.	1 in.
Curing Time, Temperature and Humitidy	28 days, 70°F 98 ± 2%	28 days, 70°F 98 ± 2%
Number of Samples	16	16

TABLE 3: DYNAMICALLY APPLIED STRESS FIELD PARAMETERS

Parameters	Model 1	Model 2
Ultimate Strength	2 to 5 ksi (Increment of 1 ksi)	2 to 5 ksi (Increment of 1 ksi)
Cyclic to Failure, N	$1,10,10^2,10^3,10^4,10^5,10^6,10^7$	$1,10,10^2,10^3,10^4,10^5,10^6,10^7$
Ratio of Maximum Applied Stress to Static Ultimate Strength, S	0.2,0.4,0.6,0.8,1.0	0.2,0.4,0.6,0.8,1.0
Coast Aggregate Shape	Round	Angular
Fine Aggregate Shape	Round	Angular
Top Size of Coarse Aggregate	1 in.	1 in.
Curing Time, Temperature, and Humidity	28 days, $70^{\circ}F$ $98 \pm 2^{\circ}F$	28 days, $70^{\circ}F$ $98 \pm 2^{\circ}F$
Number of Samples	16	16

Loading Device:

The loading device for applying Axial compressive stress is shown in Figure 1. For the Biaxial compressive stress the axial loading device was utilized in conjunction with a compressive strain gage device and the stress was applied in the X and Y direction. As for the Dynamic stress field a typical fatigue apparatus was used in which the specimen was clamped at the ends and allowed to progress through various fatigue cycles.

Concrete Specimens Under Axial Stress Fields:

Plain Concrete:

In viewing plain or reinforced concrete containing rounded or angular aggregate using the SEM under a magnification of 40,000X under stress levels of 0, 15, 30, 45, 60, and 75 percent of f'_c the failure mechanism seems to be the same regardless of the strength of concrete (hence 2, 3, 4, or 5,000 psi).

Shrinkage microcracks were found to exist in plain concrete containing rounded aggregate prior to application of compressive stress fields. These shrinkage microcracks actually encircled the aggregate particle and under applications of compressive stress fields ultimately caused the failure of the concrete specimen. At an axial compressive stress field of 15 percent of the ultimate strength of concrete (f'_c) was applied to the plain concrete containing rounded aggregate, these shrinkage microcracks widened slightly (thus, becoming bond microcracks) and it was noticed that

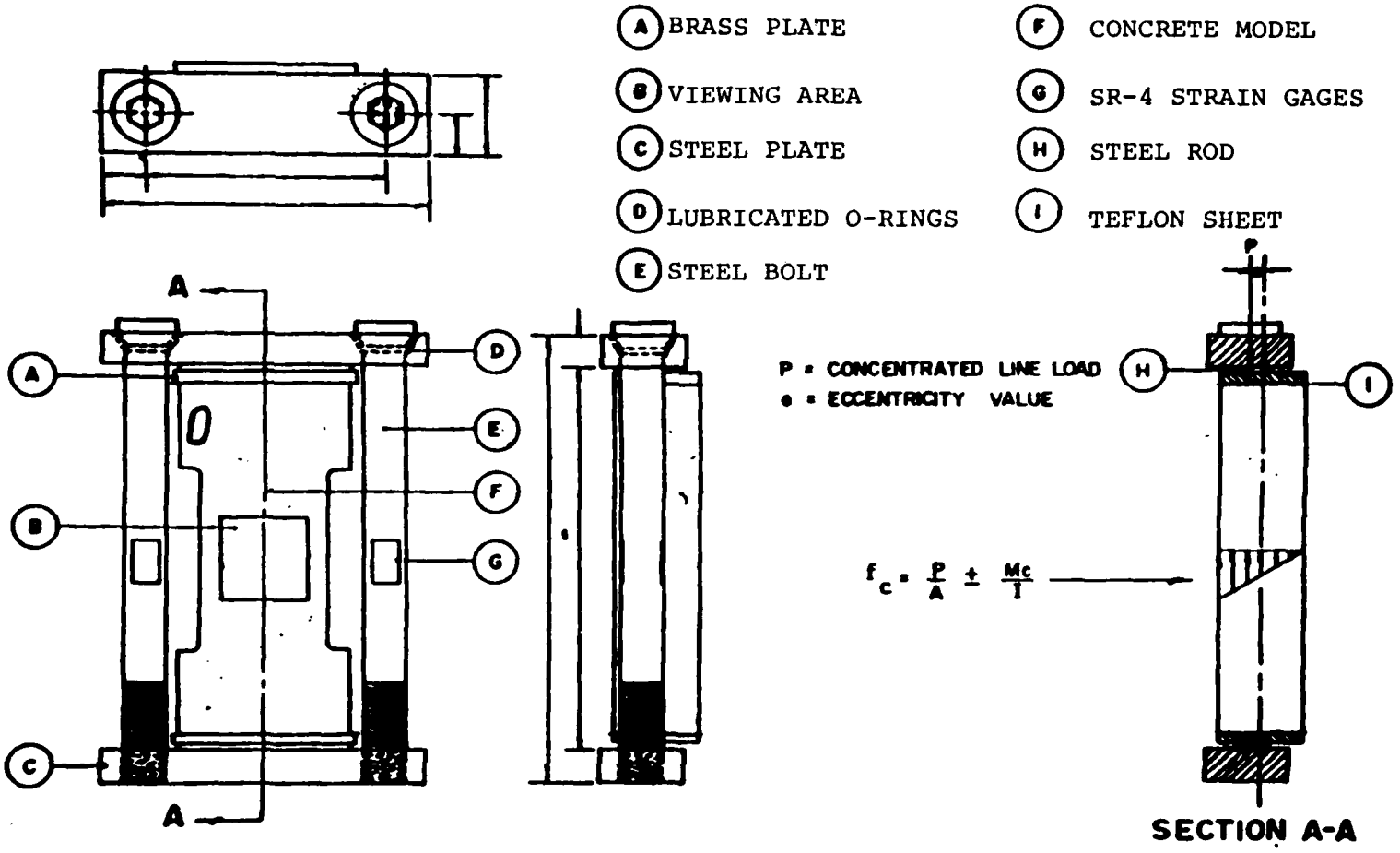

A TYPICAL LOADING APPLICATION DEPENDING ON THE CHAMBER SIZE OF THE SEM

in plotting the stress-strain curve the concrete remained elastic which indicates that concrete does have a straight line portion. However, after the axial compressive stress field was increased, the straight line portion deviated from linearity greatly. A further increase in the axial stress field to 30 percent of f'_c for plain concrete containing rounded aggregate these bond microcracks entered at right angles into the matrix (thus, forming matrix microcracks). A further increase of the axial stress field to 45 percent of f'_c resulted in complete bridging of the bond microcracks. At 60 percent of f'_c bridging of the matrix microcracks began and was completed at 75 percent of f'_c. In addition, some of the aggregate particles began to develop microcracks setting the stage for ultimate failure.

The failure pattern of plain concrete containing angular aggregate was thought to be the same as plain concrete containing rounded aggregate; however, this is not the case. Shrinkage microcracks did exist in plain concrete prior to application of compressive stress fields. However, they occurred along the smooth edge of the aggregate and do not encircle the aggregate but disappear or discontinue at points of irregularity. However, these shrinkage microcracks do ultimately lead to concrete failures. Thus, this difference may account for the fact that concrete containing angular aggregate is more durable; and one for one exhibits greater strength then concrete containing rounded aggregate. These shrinkage microcracks in plain concrete containing angular aggregate did not begin to widen until

30 percent of f'_c. Further, upon propagating, they stopped at an angular aggregate point without further circling the aggregate particle. As the compressive stress field was increased to 45 percent of f'_c the microcrack at the aggregate tip begins to extend into the matrix at various angles (unlike the right angle of plain concrete containing rounded aggregate). As the axial compressive stress field is increased to 60 percent of f'_c bridging of aggregate tips began and at 75 percent of f'_c the matrix is only 50 percent bridged. Thus, considerable more loading needs to be placed upon the specimen to cause failure. A typical failure pattern is shown in Figure 2: Failure Mechanism of Concrete.

Reinforced Concrete:

Shrinkage microcracks were found to exist in reinforced concrete in much the same manner as in plain concrete containing rounded or angular aggregate. However, it was also found that shrinkage microcracks also existed along the reinforcement. In spite of the similarity in the pattern of shrinkage microcracks, the mold of failure was different as one would expect. First, it was impossible to develop a satisfactory stress-strain curve for reinforced concrete since most of the stress was picked up by the reinforcement. The shrinkage microcracks around the reinforced concrete containing rounded aggregate did not start to widen until 45 percent of f'_c. At 60 percent of f'_c these bond microcracks began to propagate into the matrix but always ended its path at the reinforcement

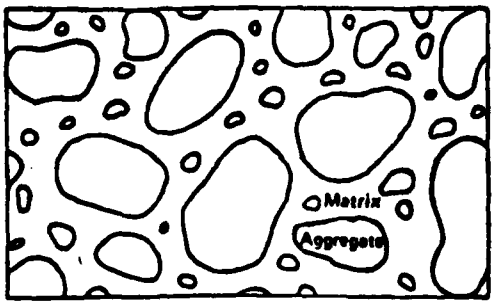

SHRINKAGE MICROCRACKS

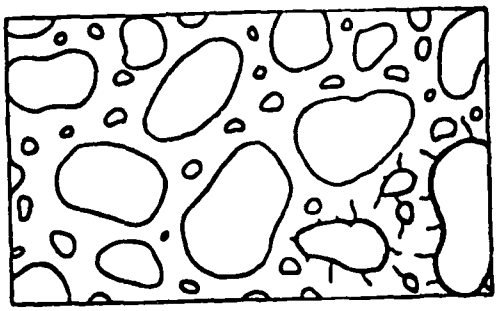

BOND MICROCRACKS

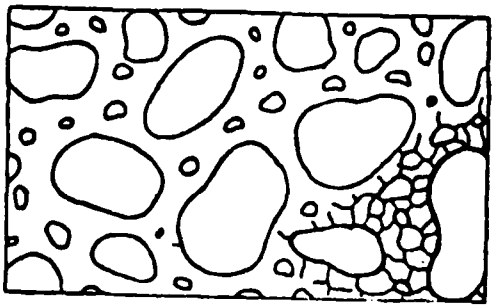

MATRIX MICROCRACKS

FAILURE MECHANISM OF CONCRETE

Figure 2

thus indicating as we know that the reinforcement was carrying the load. At 75 percent of f'_c the shrinkage microcracks along the reinforcement began to widen but no matrix imcrocrack bridging occurred.

Reinforced concrete containing angular aggregate behaves much the same way as reinforced concrete containing rounded aggregate but higher stress fields were needed to obtain the same results.

Concrete Subjected to Biaxial Stress Fields:

Plain Concrete:

In viewing plain or reinforced concrete containing rounded or angular aggregate subjected to biaxial stress fields using the SEM under a magnification of 40,000X the failure mechanism seems to be the same regardless of the strength of concrete (hence 2, 3, 4, or 5000 psi).

Obviously, shrinkage microcracks were found to exist in the plain concrete for this was no more than the same specimen type as used for concrete specimens under axial stress fields. However, this is where the simularity ends. Plain concrete containing rounded aggregate under a biaxial stress field of 15 percent of f'_c in both directions seem only to widen the existing shrinkage microcracks which surround the aggregate particle. Even at 30 percent of f'_c there appears to be no extension of these bond microcracks into the matrix but again they just widen around the

the aggregate. It would appear that the stresses more or less offset one another and compromise by widening the bond microcracks. However, this situation changes when the biaxial stress field is increased to 45 percent of f'_c. The bond microcracks extend into the matrix at various angles between 30^o and 60^o with the most common at 45^o. At this level of stress there is no increase in the size of the bond microcracks but the additional stress is alleviated as matrix microcracks. Probably the reason various angles of extension are received may be due to the rounded aggregate and/or the unevenness of the applied stress field. As the biaxial stress field is increased to 60 percent of f'_c the matrix microcracks bridge the bond microcracks and thus alleviate the additional stress. At 75 percent of f'_c the matrix microcracks begin to bridge one another and failure starts to occur. However, this seems to do so at right angles to the existing matrix microcracks.

For concrete containing angular aggregate the failure pattern is somewhat different at the higher stress levels. Again shrinkage microcracks do exist. However, no change occurs in these shrinkage microcracks at 15 percent, 30 percent, or 45 percent of f'_c. However, what does change at 45 percent of f'_c is that a microcrack starts to appear at the tip of the angular particles. (Where there is a sharp edge there appears a microcrack). Thus, it becomes apparent that the weakest point in plain concrete containing angular aggregate is the sharp edges rather than the bond (which is the

condition for plain concrete containing rounded aggregate). As the stress field is increased to 60 percent of f'_c these tip microcracks continue to propagate into matrix but at 45^o to the aggregate. In addition, the shrinkage microcracks which exist along the flat portion of the angular aggregate widen and propagate extending into the matrix also at 45^o to the aggregate. At 75 percent of f'_c the bridging of matrix microcracks start. Here we took a chance and went to 85 percent of f'_c and found that the bridging was nearing completed. But the matrix when bridged with themselves were at right angles. In addition, some of the smaller aggregate particles started to exhibit microcracks but within the aggregate these microcracks were along planes of normal failure as would be expected.

Reinforced Concrete:

The failure mechanism of reinforced concrete subjected to biaxial stress fields is considerably different than the failure mechanism of plain concrete subjected to biaxial stress fields. It appears that the reinforcement picks up a considerable amount of the stress in each direction. If a section of the reinforced concrete specimen is viewed at a location where no reinforcement occurs the failure mechanism is the same as just described. However, in viewing the specimen at the reinforcing point the failure pattern is unique. Again it is mentioned that shrinkage microcracks exist as one would expect and based on previous investigation. Further, these shrinkage

microcracks not only exist around the aggregate particles but also around the reinforcement. In viewing reinforced concrete containing rounded aggregate under a biaxial stress field of 15 percent of f'_c no apparent change in the shrinkage microcracks are evident. The same holds true at 30 percent and 45 percent of f'_c. This definitely indicates that the reinforcement is picking up most of the stress. At 60 percent of f'_c the bond microcracks (shrinkage) extends into the matrix at 45^o at the reinforcement and straight line area of the aggregate. In addition, the sharp edge of the reinforcement tends to show microcrack development. At a biaxial stress field of 75 percent of f'_c the bridging of the matrix microcracks begins but there is no evidence of failure.

Reinforced concrete containing angular has a similar pattern of failure as reinforced concrete containing rounded aggregate. There appears to be no apparent change in the shrinkage microcracks at or under a biaxial stress field of 15, 30, and 45 percent of f'_c. At 60 percent of f'_c the shrinkage microcracks extend into the matrix at 45^o and tip microcracks start to form with the straight line portion of the angular aggregate starting to extend microcracks into the matrix. At 75 percent of f'_c the bridging of the microcracks start to take place.

Concrete Specimens Under Dynamically Applied Stress Fields:

Plain Concrete:

In viewing plain or reinforced concrete containing rounded or angular aggregate under dynamically applied stress fields utilizing the SEM at a magnification of 40,000X the failure mechanism seems to be the same regardless of the strength of concrete (i.e., 2, 3, 4, or 5,000 psi). Again it is mentioned that all the concrete specimens contained shrinkage microcracks prior to application of compressive stress fields. Plain concrete containing rounded aggregate was subjected to a fatigue test at various cycles (1, 10, 10^2, 10^3, 10^4, 10^5, 10^6 and 10^7). The plain concrete containing rounded aggregate failed to survive to 10^6 and 10^7 cycles. Very little occurred to the concrete at cycles of 1, 10, 10^2 and 10^3. The shrinkage microcracks appeared to be unchanged up through cycle 10^2. When viewed at the end of cycle 10^3 the shrinkage microcracks basically widened and propagated into the matrix at right angles as experienced under the axial test. At cycle 10^4 the bridging of the matrix microcracks was completed and at cycle 10^5 the matrix microcracks appeared to be at the point of failure. Cycles 10^6 and 10^7 were never investigated because the specimens failed before the compeltion of cycle 10^6.

In viewing plain concrete containing angular aggregate the failure pattern was about the same. The concrete specimens failed to survive cycle 10^6 and thus the results at cycle 10^6 and 10^7 are not known. Again little occurred to the concrete containing

angular aggregate at cycles 1, 10, 10^2 and 10^3. The shrinkage microcracks were unchanged up through cycle 10^3. At the completion of cycle 10^4 the shrinkage microcracks entered into the matrix again at right angles. At the completion of cycle 10^5 bridging of the matrix microcracks was just about complete. The concrete did not survive cycle 10^6 although it was very close. The concrete containing rounded aggregate failed in the early stages of the start of cycle 10^6.

Reinforced Concrete:

Reinforced concrete containing rounded aggregate survived just prior to cycle 10^6 whereas reinforced concrete containing angular aggregate survived just beyond cycle 10^6. The odd part about the reinforced concrete containing rounded or angular aggregate was that basically very few signs of failure were evident until the cycle before failure. Thus, no great change in shrinkage, bond, or matrix microcracks was that evident. This is to say the pattern observed in concrete subjected to axial or biaxial stress fields was not observed here.

INVESTIGATION AND RESULTS (PHASE II - YEAR 2)

General:

The results of Phase I - Year 1 have shown that the SEM is an invaluable tool for the investigation of concrete for both plain and reinforced concrete when subjected to various stress fields and loading conditions (axial, biaxial, and dynamic). However, Phase I - Year 1 of this investigation concerned itself mainly with the failure mechanism of general concrete. By the term general concrete, it is meant that concrete made of or consisting of the five basic concrete making materials (portland cement, water, air, fine and coarse aggregate). The failure mechanism of concrete containing additional additives was not investigated in the Phase I - Year 1 project. Thus, a phase II - Year 2 project was initiated and completed utilizing the results obtained in Phase I - Year 1 to obtain information on the formation and propagation of microcracks in concrete made with a blended cement for both plain and reinforced concrete both before and after applications of axial, biaxial, and dynamic stress fields utilizing the SEM. In each case the blended cement consisted of a 15 percent replacement material. These additives utilized were pozzolan or fly ash (15 percent), fly ash-lime (10 - 5 percent), and fly ash-lime-sulphur (5-5-5 percent). Again as in Phase I - Year 1 some information regarding microcracks, propagation of these microcracks (concrete fracture), aggregate shape, plain

and reinforced concrete, the sum effects of the various stress fields, and the ultimate strength of concrete was found.

Scanning Electron Microscope:

Again as in Phase I - Year 1 the results have shown that the SEM at 40,00X magnification is an invaluable tool for the investigation of both plain and reinforced concrete made with a blended cement when subjected to various stress fields and loading conditions (axial, biaxial, and dynamic).

Concrete Specimens:

Two distinct concrete models of each condition and for each stress field (axial, biaxial, and dynamic) were utilized. These additives consisted of pozzolan or fly ash (15 percent replacement), fly ash-lime (10 - 5 percent replacement), and fly ash-lime-sulphur (5-5-5 percent replacement). Thus, each additive and/or combinations of additives were utilized as a cement replacement in the amount of 15 percent by weight of cement. The following parameters were used.

Approximately 2, 3, 4, and 5 ksi concrete was used to form twenty four beams 3 X 3 X 14 in. (twelve plain and twelve reinforced) for each of the stress field parameters considered (axial, biaxial, and dynamic). (See Table 4, 5 and 6.) In addition, of the twelve beams six contained rounded aggregate and six contained angular aggregate. In the twelve reinforced beams six contained

TABLE 4: AXIAL STRESS FIELD PARAMETERS CONSIDERED FOR BLENDED CEMENTS

Parameters	Model 1	Model 2
Ultimate Strength	2 to 5 ksi (Increments of 1 ksi)	2 to 5 ksi (Increments of 1 ksi)
Axial Stress Fields	15, 30, 45, 60, 75%	15, 30, 45, 60, 75%
Coarse Aggegate Shape	Rounded	Angular
Fine Aggregate Shape	Rounded	Angular
Top Size of Coarse Aggregate	1 in.	1 in.
Curing Time, Temperature and Humidity	28 days, 70°F 98 $\pm$ 2%	28 days, 70°F 98 $\pm$ 2%

This was the pattern for all three admixtures and/or blended cements.

TABLE 5: BIAXIAL STRESS FIELD PARAMETERS CONSIDERED FOR BLENDED CEMENTS

Parameters	Model 1	Model 2
Ultimate Strength	2 to 5 ksi (Increments of 1 ksi)	2 to 5 ksi (Increments of 1 ksi)
Stress Field in the x direction	15, 30, 45, 60, 75%	15, 30, 45, 60, 70%
Stress Field in the y direction	15, 30, 45, 60, 75%	15, 30, 45, 60, 70%
Coarse Aggregate Shape	Rounded	Angular
Fine Aggregate Shape	Rounded	Angular
Top Size of Coarse Aggregate	1 in.	1 in.
Curing Time, Temperature, and Humidity	28 days, 70% 98 $\pm$ 2%	28 days, 70% 98 $\pm$ 2%

This was the pattern for all three admixtures and/or blended cements.

TABLE 6: DYNAMICALLY APPLIED STRESS FIELD PARAMETERS CONSIDERED FOR BLENDED CEMENTS

Parameters	Model 1	Model 2
Ultimate Strength	2 to 5 Ksi (Increments of 1 Ksi)	2 to 5 Ksi (Increments of 1 Ksi)
Cyclic to Failure, N	$1,10,10^2,10^3,10^4,10^5,10^6,10^7$	$1,10,10^2,10^3,10^4,10^5,10^6,10^7$
Coarse Aggreagate Shape	Round	Angular
Fine Aggregate Shape	Round	Angular
Top Size of Coarse Aggregate	1 in.	1 in.
Curing Time, Temperature and Humidity	28 days, $70^{\circ}F$ 98 $\pm$ 2%	28 days, $70^{\circ}F$ 98 $\pm$ 2%

This was the pattern for all three admixtures and/or blended cements.

rounded aggregate and six contained angular aggregate. Three specimens were sawed from each beam for a total of 72 specimens (36 containing rounded aggregate (18 plain and 18 reinforced) and 36 containing angular aggregate (18 plain and 18 reinforced)). Each beam was cured for 28 days at 70°F and 98 ± 2% relative humidity. After the 28 days of curing, the specimens were sawed from each beam using a diamond blade saw. The face of each specimen was polished using a silicon-carbide slurry on a jewelers wheel. The specimens were than squared by use of a surface grinder.

Loading Devices:

The loading devices for the Phase II - Year 2 were the same as used in the Phase I - Year 1 study.

Concrete Specimens Under Axial Stress Fields:

Plain Concrete:

In viewing plain or reinforced concrete made with blended cements containing rounded or angular aggregate using the SEM under a magnification of 40,000x under stress levels of 0, 15, 30, 45, 60, and 75 percent of f'_c the failure mechanism seems to be the same regardless of the strength of concrete (hence 2, 3, 4 or 5000 psi). However, the failure mechanism is not the same pattern for the three mixtures of blended cement. Thus, the failure pattern is different for concrete containing a pozzolan (15%) versus pozzolan lime (10 - 5%) versus pozzolan - lime-sulphur

(5-5-5%).

Shrinkage microcracks were found to exist in plain concrete made with blended cements containing rounded aggregate prior to application of compressive stress fields. However, depending on the type or mixture of blended cement these shrinkage microcracks varied in size. The concrete made with 15 percent pozzolan (fly ash) exhibited a much smaller ring around the aggregate particles. In fact it was difficult to determine if shrinkage microcracks did exist. When compared to the concrete specimens made with normal cement (Phase I - Year 1), which is difficult to do, one sees that the concrete made with blended cement (85% cement - 15% fly ash) exhibits shrinkage microcracks in width about one-half the normal cement concrete.

In viewing shrinkage microcracks in concrete made with a blended cement of the combination fly ash and lime (85% cement, 10% fly ash, and 5% lime) a different picture results. In this case the addition of the added ingredients did not alter the size of the shrinkage microcrack when compared to concrete made with normal cement.

Concrete made with a blended cement of fly ash-lime-sulphur (85% cement, 5% fly ash, 5% lime, 5% sulphur) performed overall very poorly. In most cases this concrete failed before a load of 70% f'_c could be reached at the lower levels and 50% f'_c at the upper levels. The shrinkage microcracks were more of a ring around the aggregate much like one would see in the alkai silica reaction.

It was extremely difficult to distinguish between microcracks or some form of bond failure due to a chemical reaction although this chemical reaction should not have taken place. Thus uncertainty results.

When the compressive stress field was increased to 15% of f'_c (the ultimate strength of concrete) for the plain concrete containing rounded aggregate there was no change in the shape or size of the shrinkage microcrack (now bond microcrack) for the concrete made with the blended cement containing 15 percent fly ash.

There was a slight change in the same type of concrete made with 15 percent fly ash-lime mixture. In this case the bond microcracks widened slightly much like one would suspect happened in the plain concrete case made with rounded aggregate using normal cement rather than blended cement.

In the case of the concrete (plain) made with rounded aggregate, and a 15 percent blended cement of fly ash-lime-sulphur no meaningful results could be obtained. It was difficult to determine if microcracks exist or if some chemical reaction had taken place. This portion of the experiment was a failure.

When the axial compressive stress field was increased to 30 percent of f'_c for plain concrete containing rounded aggregate made with a blended cement of 15 percent fly ash the results were similar to concrete made with normal cement under a compressive stress field of 15 percent. Thus, these bond microcracks (initially shrinkage microcracks) just widened with one or two off shoots into the matrix

at right angles.

In the case of the concrete made with the fly ash-lime mixture under an application of 30 percent f'_c the bond microcracks widened and began to enter the matrix at right angles to the microcracks thus forming a matrix microcrack.

Increasing the axial compressive stress field to 45 percent of f'_c the concrete containing the blended cement of 15 percent fly ash resulted in the bond microcracks entering into the matrix at right angles. In the case of the concrete containing the fly ash-lime blended cement under an axial compressive stress field of 45 percent of f'_c resulted in complete bridging of the bond microcracks.

At 60 percent of f'_c bridging of the bond microcracks was completed for the blended cement containing 15 percent fly ash and the bridging of the matrix microcracks was completed for the blended cement containing fly ash-lime (10 - 5 percent).

At 75 percent of f'_c bridging was completed for all concretes and there was some small evidence of aggregate fragmentation setting the stage for ultimate failure.

Again the failure pattern for plain concrete (as opposed to reinforced concrete) containing angular aggregate made with blended cements follows a similar failure policy. The concrete containing angular aggregate is more stable and durable whether it is made with blended cements in comparing it to its counterpart (concrete containing rounded aggregate). Here again shrinkage

microcracks do exist; but, along the smooth surface of the aggregate and appear not to surround the aggregate. When there is a sharp break or point in the aggregate the crack goes off into the matrix somewhat.

In the case of concrete made with blended cement containing angular aggregate the fly ash-lime-sulphur (5-5-5) admixture was a failure and its best not to mention it at all. In the other two cases the pattern is as follows. In the concrete containing the fly ash-lime mixture the pattern was the same as if the concrete was made with 100 percent normal cement. In the concrete with angular aggregate containing blended cement in the form of 15 percent fly ash the results were somewhat difficult. In this particular case the results followed that of its counterpart containing rounded aggregate. It was impossible to judge any difference in the results. It is possible to assume that if the 15 percent increase in applied stress were reduced some difference would be noticed.

Reinforced Concrete:

Shrinkage microcracks were found to exist in reinforced concrete in much the same manner as in plain concrete containing rounded or angular aggregate made with blended cements. In addition, these shrinkage microcracks also existed along the reinforcement.

Again it should be mentioned that the results of concrete made with a blended cement of the fly ash-lime-sulphur mixture is not worth reporting. Again it appears that some type of chemical reaction had taken place in which a rim appeared around the aggregate thus making it difficult to distinguish microcracks from flaws or whatever.

First looking at the concrete made with a blended cement of 15 percent fly ash as the additive; the shrinkage microcracks around the reinforced concrete containing rounded aggregate did not start to widen until 45 percent of f'_c and here it was only slight. In a few cases there were off-shoots into the matrix and in so doing they would end at the reinforcement. When the stress was increased to 60 percent of f'_c these bond microcracks propagated slightly into the matrix but did not seem to effect the bond-matrix structure or weaken it to any extent. At 75 percent of f'_c the matrix microcracks were running from aggregate to aggregate or aggregate to reinforcement. However, the bridging was just started and by no means completed.

Viewing the same type of concrete made with the fly ash blended cement: but, instead of rounded aggregate we have angular aggregate the results are the same. It appears the reinforcement picks up most of the load.

If we now turn our attention to the concrete made with a blended cement of fly ash-lime (10 - 5 percent) as the additive; the shrinkage microcrack pattern as well as its propagation and failure made is the same as if the concrete was made of a non blended cement.

The failure pattern holds true for that concrete made with the same blended cement (fly ash-lime) with angular aggregate.

Concrete Subjected to Biaxial Stress Fields:

Plain Concrete:

In viewing plain or reinforced concrete made with blended cements containing rounded or angular aggregate subjected to biaxial stress fields using the SEM under a magnification of 40,000x the failure mechanism can be said to be the same for all practical purposes regardless of the strength of concrete (2, 3, 4 or 5 ksi).

It is apparent that all concrete throughout this study contains shrinkage microcracks regardless of the cement type, water cement ratio, or aggregate shape.

It should be further pointed out that the concrete made with the blended cement of fly ash-lime-sulphur is not worth discussion for no significant results were obtained.

First we will present the results of plain concrete subjected to a biaxial stress field made with a blended cement of 15 percent fly ash and containing rounded aggregate. This particular group of specimens were subjected initially to a biaxial stress field of 15 percent of f'_c in both directions (x and y). Basically nothing happened at 40,000x magnification. There was no change in the shrinkage microcrack pattern. Even under a biaxial stress field of 30 percent of f'_c in both directions very little happened.

There was no extension of the microcracks into the matrix. The width of the microcrack changed slightly. It begins to appear that the stresses more or less offset one another and somehow compromise by just widening the shrinkage or bond microcrack. Even at a biaxial compressive stress field of 45 percent of f'_c the bond microcracks slightly extended into the matrix at various angles. As the biaxial stress field is increased to 60 percent of f'_c the matrix microcracks begin to bridge the bond microcracks. Finally at 75 percent of f'_c the matrix microcracks begin to bridge one another and again do so at right angles.

In comparing the results as obtained in the above, with concrete made with a blended cement of fly ash-lime, not much change occurs. The only difference occurs at the 60 and 75 percent levels. At 60 percent of f'_c under a biaxial stress field the matrix microcracks bridge the bond microcracks totally and at 75 percent of f'_c under a biaxial stress field the matrix microcrack bridging is completed.

Going one step further with the plain concrete (unreinforced) subjected to biaxial stress fields with the two types of blended cements containing angular aggregate the results are somewhat different. First looking at the concrete containing blended cement with just fly ash no serious changes occur until 60 percent of f'_c in each direction. At that point the bond microcracks (initial shrinkage microcracks) begin to propagate into the matrix and at 75 percent of f'_c in each direction the bridging of the bond micro-

cracks are completed. The exception occurs when there is a large irregularity or point within the aggregate. At this point it appears to act as a release value and the microcracks are propagated from this point at various angles.

When one views the situation in which the blended cement is fly ash-lime (10 - 5 percent) this with angular aggregate reacts much in the same manner as plain concrete (unreinforced) made with normal cement (100 percent) containing angular aggregate. Thus, at 45 percent of f'_c in each direction a microcrack starts to appear at points of irregularity (sharp edges). As the biaxial stress field increases to 60 percent of f'_c these microcracks propagate into the matrix and at 75 percent of f'_c the bridging is completed.

Reinforced Concrete:

The failure mechanism of reinforced concrete subjected to biaxial stress fields like that of that of concrete subjected to axial stress fields is considerably different than the failure mechanism of plain concrete subjected to biaxial or axial stress fields. The reason for this is that the reinforcement picks up a considerable amount of the load or it appears as if it does. Again shrinkage microcracks exist around the aggregate (rounded or angular) and also around or along the reinforcement. If one views that concrete containing rounded aggregate made with the blended cement containing just the fly ash, very little is affected. No action or microcrack propagation occurs at 15, 30, 45,

or 60 percent of f'_c in both directions. At 75 percent of f'_c in both directions the bond microcracks (initial shrinkage microcracks) extend into the matrix and seem to extend until a point of relief at the reinforcement.

The specimens of similar nature but made with a blended cement of fly ash-lime (10 - 5 percent) show no apparent changes at 15, 20, or 45 percent of f'_c in both directions. At 60 percent of f'_c the bond microcracks extends into the matrix at 45^o at the reinforcement and smooth surfaces of the aggregate. At a biaxial stress field of 75 percent of f'_c the bridging of the matrix microcracks begins but there is no evidence of failure.

Reinforced concrete containing angular aggregate has a similar pattern of failure as reinforced concrete containing rounded aggregate.

Concrete Specimens Under Dynamically Applied Stress Fields:

Plain Concrete:

In viewing plain or reinforced concrete made with blended cements containing rounded or angular aggregate under dynamically applied stress fields utilizing the SEM at a magnification of 40,000x the failure mechanism seems to be the same regardless of the strength of concrete (2, 3, 4, or 5 ksi). Again, it is mentioned that all concrete specimens contained shrinkage microcracks prior to application of any stress fields (axial, biaxial, or dynamic).

The plain concrete rounded aggregate and made with the 15 percent fly ash blended cement failed to survive the 10^6 cycles. There was no change in the shrinkage microcracks (bond microcracks) through the 10^4 cycles. At this point the shrinkage microcracks widened considerably and began to propagate into the matrix. At 10^5 cycles the corners of the specimen sheared off and shortly after that the specimens failed altogether. In the specimens of the same material but containing angular aggregate the results were much the same, just a repeat.

In the case of plain concrete containing rounded aggregate and made with the fly ash-lime (10 - 5 percent) blended cement these specimens failed between 10^5 and 10^6 cycles. Again little change took place after each cyle up to 10^4. At this point the shrinkage microcracks (now bond microcracks) widened. After that failure started to occur rapidly and no meaningful results were obtained. The pattern held true for the specimens at levels containing angular aggregate.

It appears that the failure in most cases was sudden and unexpected from the conditions associated with the concrete. It was also surprising that strength of the concrete didn't play a bigger role in the failure mechanism under dynamic loading.

Reinforced Concrete:

The reinforced concrete specimens regardless of material used; blended cements, or aggregate sized continued to last somewhat longer

up to 10^6 and sometimes 10^7 cycles. However, it became impossible to distinguish microcracks from reinforcement from peaks and valleys. Changing set in when using the SEM and viewing became impossible. Again it was surprising that concrete strength didn't play a bigger role in the dynamic effects.

INVESTIGATION AND RESULTS (PHASE III - YEAR 3)

General:

The third year of this investigation dealt mostly with a state-of-the-art approach in searching out a series of equations that might be utilized to predict failure. Thus, the model chosen for the analysis was a numerical matching method which was first reported by Professor H.D. Conway and written into a Ph.D. dissertation by T.T.C. Hsu; Microcracks in Concrete, Cornell University, 1962. This type of an analysis of a model can be used for any material made up of particles of one substance, cemented together by a second substance, and subjected to differential volume change. In particular, it was used for concrete subjected to any kind of volume change, such as shrinkage or expansion due to wetting and drying, temperature change, and especially hydration. Since this portion of the investigation was more of a literature search to seek out an appropriate method, I have included Dr. Hsu results and discussion.

Stress Analysis:

Stress analysis was made on the model as shown in Fig. 3. Take the coordinate as shown. Due to the symmetry about the X-axis, Y-axis and 45 degrees axis, it is only necessary to consider the stresses in the area bounded by OA2C. See Fig. 4.

When the paste-mortar shrinks, the aggregate particles will move toward each other. It is first assumed that these particles are fixed in space. In this state, the stress in the paste-mortar is constant throughout, and equal to:

$$\sigma_1 = \frac{E}{1 - \nu} \varepsilon \qquad (1)$$

where ε is the known free shrinkage strain of the paste-mortar, E its modulus of elasticity, and ν its Poisson's ratio. A uniform normal stress is set up along the line OA, while the shear stress equals zero due to symmetry. The system is then released and the aggregates permitted to move toward each other, i.e. points A, O will move to A', O' respectively. Because of symmetry, O'A' will remain a straight line parallel to OA. A stress field $\sigma_2(x,y)$ is induced by the relaxation of the system, whose intensity is directly proportional to the displacement AA' = K. The unknown k is indirectly governed by the equilibrium condition for residual stresses

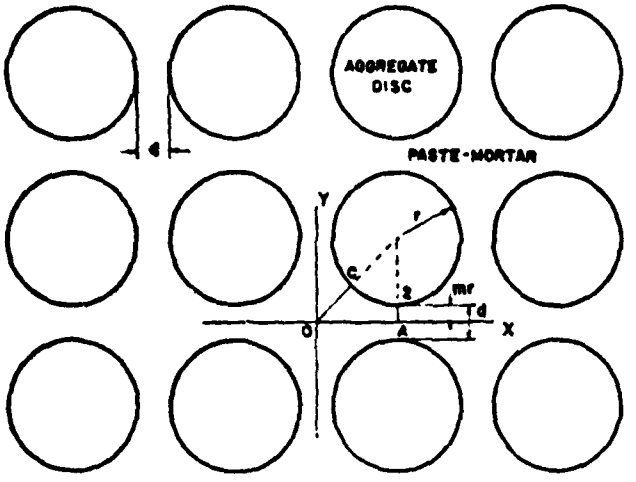

FIG. 3

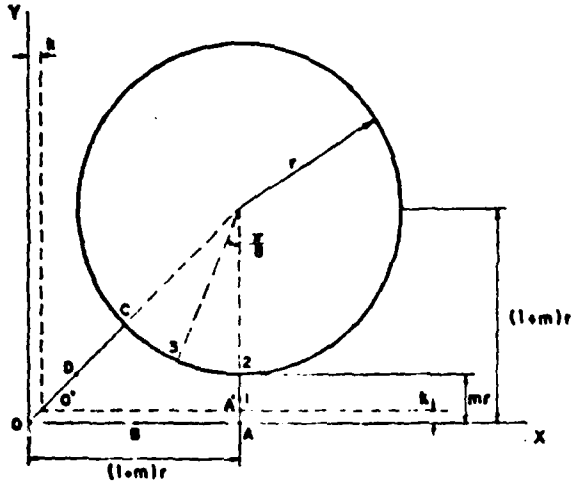

FIG. 4

in the absence of external loads, i.e. the summation of vertical stresses on the face O to A must be zero. The summation includes σ_{2y}, and σ_1, which is constant from O to A. The length from O to A is (1+m)r. Thus,

$$\int_O^A \sigma_{2y}\, ds + \sigma_1(1+m)r = 0 \qquad (2)$$

where $\sigma_{2y} \int_O^A$ is the normal stress on the face O to A. The final stress at each point is then:

$$\sigma_F(x,y) = \sigma_1 + \sigma_2(x,y) \qquad (3)$$

The problem is to find $\sigma_2(x,y)$. This is achieved by using a stress function F.

The stress function F must satisfy the usual plane stress equation to ensure compatibility,

$$\left(\frac{\partial^2}{\partial x^3} + \frac{\partial^2}{\partial y^2}\right)\left(\frac{\partial^2}{\partial x^3} + \frac{\partial^2}{\partial y^2}\right) F = 0 \qquad (4)$$

Let $F = \psi(y) \sin x$ or $\psi(y) \cos x$ and substitute into equation (4)

$$\psi - 2\alpha^2\psi'' + \alpha''\psi = 0$$

Let $\psi(y) = e^{\lambda x}$,

$$\lambda^4 - 2\alpha^2\lambda^2 + \alpha^4 = 0$$

$$(\lambda^2 - \alpha^1)^2 = 0$$

$$\lambda = \pm\alpha$$

$$\psi = A\, e^{\alpha y} + B\, e^{-\alpha y} + C\alpha y\, e^{\alpha y} + D\alpha y\, e^{-\alpha y}$$

$$\text{or } A \sinh\alpha y + B \cosh\alpha y + C\alpha y \sinh\alpha y + D\, \alpha y \cosh\alpha y$$

Choose the hyperbolic sine and cosine for convenience; the general form of F is:

$$\begin{aligned} F = &\sum_n (A_n \sinh\alpha_n y + B_n \cosh\alpha_n y + C_n d_n y \sinh\alpha_n y + D_n \alpha_n y \cosh\alpha_n y) \sin\alpha_n x \\ &+ \sum_n (E_n \sinh\alpha_n y + F_n \cosh\alpha_n y + C_n \alpha_n y \sinh\alpha_n y + H_n \alpha_n y \cosh\alpha_n y) \cos\alpha_n x \\ &+ \sum_n (I_n \sinh\alpha_n x + J_n \cosh\alpha_n x + K_n \alpha_n x \sinh\alpha_n x + L_n \alpha_n x \cosh\alpha_n x) \sin\alpha_n y \\ &+ \sum_n (M_n \sinh\alpha_n x + N_n \cosh\alpha_n x + P_n \alpha_n x \sinh\alpha_n x + Q_n \alpha_n x \cosh\alpha_n x) \cos\alpha_n y \end{aligned}$$

Due to the symmetry about the X and Y axes, the terms $\sin\alpha_n x$, $\sin\alpha_n y$, $\sinh\alpha_n x$, $\sinh\alpha_n y$, $\alpha_n x \cosh\alpha_n x$, and $\alpha_n y \cosh\alpha_n y$ drop out,

$$\begin{aligned} F = &\sum_n (A_n \cosh\alpha_n y + B_n \alpha_n y \sinh\alpha_n y) \cos\alpha_n x \\ &(C_n \cosh\alpha_n x + D_n \alpha_n x \sinh\alpha_n x) \cos\alpha_n y \end{aligned}$$

Due to the symmetry about the 45 degree axis,

$$A = C, \qquad B = D,$$

and $F = \sum_n A_n(\cosh\alpha_n y \cos\alpha_n x + \cosh\alpha_n x \cos\alpha_n y)$

$+ \sum_n B_n(\alpha_n y \sinh\alpha_n y \cos\alpha_n x + \alpha_n x \sinh\alpha_n x \cos\alpha_n y)$ (5)

Thus,

$$\alpha_x = \frac{\partial^2 F}{\partial y^3} = \sum_n A_n\alpha_n^2(\cosh\alpha_n y \cos\alpha_n x - \cosh\alpha_n x \cos\alpha_n y)$$
$$+ \sum_n B_n\alpha_n^2(\alpha,y \sinh\alpha_n y \cos\alpha_n x - d_n x \sinh\alpha_n x \cos\alpha_n y$$
$$+ 2\cosh\alpha_n y \cos\alpha_n x) \quad (6)$$

$$\alpha_y = \frac{\partial^2 F}{\partial x^2} = \sum_n A_n\alpha_n^2(-\cosh\alpha_n y \cos\alpha_n x - \cosh\alpha_n x \cos\alpha_n y)$$
$$+ \sum_n B_n\alpha_n^2(-\alpha,y \sinh\alpha_n y \cos\alpha_n x - \alpha_n x \sinh\alpha_n x \cos\alpha_n y$$
$$+ 2\cosh\alpha_n y \cos\alpha_n y) \quad (7)$$

$$\tau_{xy} = \frac{\partial^2 F}{\partial x \partial y} = \sum_n A_n\alpha_n^2(\sinh\alpha_n y \sin\alpha_n x + \sinh\alpha_n x \sin\alpha_n y)$$
$$+ \sum_n B_n\alpha_n^2(\alpha_n y \cosh\alpha_n y \sin\alpha_n x + \alpha_n x \cosh\alpha_n x \sin\alpha_n y$$
$$+ \sinh\alpha_n y \sin\alpha_n x + \sin\alpha_n x \sin\alpha_n y) \quad (8)$$

Let u : displacement in X direction,

v : displacement in Y direction,

$$u = \int \varepsilon_x d_x + C_1(y) + C_1 = \frac{1}{E}\int(\alpha_x - \nu\alpha_y)\,dx + C_1(y) + C_2$$
$$= \sum_n A_n\alpha_n(1+\nu)(\cosh\alpha_n y \sin\alpha_n y - \sinh\alpha_n x \cos\alpha_n y)$$
$$+ \sum_n B_n\alpha_n[(1+\nu)\alpha_n y \sinh\alpha_n y \sin\alpha_n x - (1+\nu)\alpha_n x \cosh\alpha_n x \cos\alpha_n y$$
$$+ (1-\nu)\sinh\alpha_n x \cos\alpha_n y + 2\cosh\alpha_n y \sin\alpha_n x] + C_1(y)$$
$$+ C_2 \quad (9)$$

$$v = \int \varepsilon_y d_y + C_3(x) + C_4 = \frac{1}{E}\int(\alpha_y - \nu\alpha_x)\,d_y + C_3(x) + C_4$$
$$= \sum_n A_n\alpha_n(1+\nu)(-\sinh\alpha_n y \cos\alpha_n x + \cosh\alpha_n x \sin\alpha_n y)$$
$$+ \sum_n B_n\alpha_n[-(1+\nu)d_n y \cosh\alpha_n y \cos\alpha_n x + (1+\nu)\alpha_n x \sinh\alpha_n x \sin\alpha_n y$$
$$+ (1-\nu)\sinh\alpha_n y \cos\alpha_n y + 2\cosh\alpha_n x \sin\alpha_n y]$$
$$+ C_3(x) + C_4 \quad (10)$$

The boundary conditions for the stress function are:

At $y = 0$,	$\tau_{xy} = 0$	(a)
	$v = k$	(b)
At $x = y$,	$\alpha_x = \alpha_y$	(c)
	$u = v$	(d)
At $x = (1+m)r$,	$u = 0$	(e)
	$\tau_{xy} = 0$	(f)
At the interface	$u = 0$	(g)
	$v = 0$	(h)

The conditions (e), (g), (h) were obtained by assuming the aggregates to be rigid.

The conditions (a) and (c) are automatically satisfied by the chosen stress function and condiitons (b) and (c) are used to determine the constant C_1, C_2, C_3, and C_4 in Eqs. (9) and (10) as follows:

When $y = 0$, $v = k$,

$$C_3(x) + C_4 = k$$

$$C_3 = 0, \text{ and } C_4 = k.$$

When $x = y$, $u = v = k$

$$C_1(y) + C_2 = C_3(x) + C_4$$

$$C_1 = C_3 = 0, \text{ and } C_2 = C_4 = k$$

In order to satisfy the remaining boundary conditions, a point matching method was used. It was anticipated that by taking five points A, C, 1, 2, and 3 (see Fig. 4) on the interface and on line $x = (1+m)r$, a good approximation could be obtained. Points A and C

each give one equation, while points 1, 2, and 3 each give two equations. There will be eight equations together with Eq. (2). Thus, nine unknowns were needed. Taking n = 4 for the stress function F provides unknowns A_1, A_2, A_3, A_4, B_1, B_2, B_3, and B_4 in addition to the unknown displacement k. Therefore nine simultaneous equations with nine unknowns are obtained as follows:

Take $\alpha_n = \frac{n\pi}{2(1+m)r^3}$,

<u>At point A</u>, $x = (1+m)r$; $y = 0$

$$\alpha_n x = \frac{n\pi}{2} = j_1 \ (n); \qquad \alpha_n y = 0$$

$$u = 0, \sum_{n=1}^{4} A_n\alpha_n(1+\nu)(\sinh j_1 - \sinh j_1)$$

$$+ \sum_{n=1}^{4} B_n\alpha_n[-(1+\nu)j_1 \cosh j_1 + (1-\nu)\sinh j_1 + 2 \sinh j_1] + EK = 0 \quad (11)$$

<u>At point C</u>, $x = y = (0.29289324+m)r$,

$$\alpha_n x = \alpha_n y = \left(\frac{0.29289324+m}{1+m}\right) \frac{n\pi}{2} = J_2(m,n)$$

$$u = 0, \sum_{n=1}^{4} A_n\alpha_n(1+\nu)(\cosh j_2 \sinh j_2 - \sinh j_2 \cos j_2)$$
$$v = 0,$$

$$+ \sum_{n=1}^{4} B_n\alpha_n[(1+\nu)j_2 \sinh j_2 \sinh j_2 - (1+\nu)j_2 \cosh j_2 \cos j_2$$

$$+(1-\nu)\sinh j_2 \cos j_2 + 2 \cosh j_2 \sinh j_2] + EK = 0 \quad (12)$$

At point 1, $x = (1+m)r$; $y = \frac{m}{2}r$;

$$\alpha_n x = \frac{n\pi}{2} = J_1(n); \quad \alpha_n y = \frac{m}{2(1+m)}\,\frac{n\pi}{2} = j_3(m,n)$$

$$\tau_{xy} = 0, \sum_{n=1}^{4} A_n\alpha_n^2(\sinh j_3 \sin j_1 + \sinh j_1 \sin j_3)$$

$$+ \sum_{n=1}^{4} B_n\alpha_n^2 (j_3 \cosh j_3 \sin j_1 + \sinh j_3 \sin j_1$$

$$+ j_1 \cosh j_1 \sin j_3 + \sinh j_1 \sin j_3) = 0 \qquad (13)$$

$$u = 0 \quad \sum_{n=1}^{4} A_n\alpha_n(1+\nu)(\cosh j_3 \sin j_1 - \sinh j_1 \cos j_3)$$

$$+ \sum_{n=1}^{4} B_n\alpha_n[(1+\nu)j_3 \sinh j_3 \sin j_1 - (1+\nu)j_1 \cosh j_1 \cos j_3$$

$$+(1-\nu)\sinh j_1 \cos j_3 + 2 \cosh j_3 \sin j_1] + EK = 0 \qquad (14)$$

At point 2, $x = (1+m)r$; $y = mr$;

$$\alpha_n x = \frac{n\pi}{2} = j_1(n); \quad \alpha_n y = \frac{m}{1+m}\,\frac{n\pi}{2} = j_4(m,n)$$

$$u = 0, \sum_{n=1}^{4} A_n\alpha_n(1+\nu)(\cosh j_4 \sin j_1 - \sinh j_1 \cos j_4)$$

$$+ \sum_{n=1}^{4} B_n\alpha_n[(1+\nu)j_4 \sinh j_4 \sin j_1 - (1+\nu)j_1 \cosh j_1 \cos j_4$$

$$+(1-\nu)\sinh j_1 \cos j_4 + 2 \cosh j_4 \sin j_1] + EK = 0 \qquad (15)$$

$$v = 0, \sum_{n=1}^{4} A_n\alpha_n(1+\nu)(-\sinh j_4 \cos j_1 + \cosh j_1 \sin j_4)$$

$$+ \sum_{n=1}^{4} B_n\alpha_n[-(1+\nu) j_4 \cosh j_4 \cos j_1 + (1+\nu) j_1 \sinh j_1 \sin j_4$$

$$+(1-\nu)\sinh j_4 \cos j_1 + 2 \cosh j_1 \sin j_4] + EK = 0 \qquad (16)$$

<u>At point 3</u>, $x = (0.61731657+m)r$; $y = (0.07612047+m)r$;

$$\alpha_n x = \left(\frac{0.61731657+m}{1+m}\right) \frac{n\pi}{2} = j_5(m,n);$$

$$\alpha_n y = \left(\frac{0.07612047+m}{1+m}\right) \frac{n\pi}{2} = j_6(m,n);$$

$$u = 0, \sum_{n=1}^{4} A_n\alpha_n(1+\nu)(\cosh j_6 \sin j_5 - \sinh j_5 \cos j_6)$$

$$+ \sum_{n=1}^{4} B_n\alpha_n [(1+\nu) j_6 \sinh j_6 \sin j_5 - (1+\nu) j_5 \cosh j_5 \cos j_6$$

$$+(1-\nu)\sinh j_5 \cos j_6 + 2 \cosh j_6 \sin j_5] + EK = 0 \qquad (17)$$

$$v = 0 \sum_{n=1}^{4} A_n\alpha_n(1+\nu)(-\sinh j_6 \cos j_5 + \cosh j_5 \sin j_6)$$

$$+ \sum_{n=1}^{4} B_n\alpha_n [-(1+\nu) j_6 \cosh j_6 \cos j_5 + (1+\nu) j_5 \sinh j_5 \sin j_6$$

$$+(1-\nu)\sinh j_6 \cos j_5 + 2 \cosh j_5 \sin j_6] + EK = 0 \qquad (18)$$

Equilibrium of stresses on face 0 to A

$$\int_0^A \alpha_{2y}\, dx + \alpha_1(1+m)r = 0, \qquad \frac{n\pi}{2} = j_1(n)$$

$$\sum_{n=1}^{4} A_n\alpha_n(-\sin j_1 + \sinh j_1) + \sum_{n=1}^{4} B_n\alpha_n(j_1 \cosh j_1 + \sinh j_1)$$

$$+ \alpha_1(1+m)r = 0 \qquad (19)$$

The numerical evaluation of the coefficients of these nine equations, the solving of the simultaneous equation, and the computation of the stresses by substituting the values of A_1 to A_4 and B_1 to B_4 into Eqns. (6), (7) and (8) were done on an electronic digital computer with the following assumptions:

(a) Poisson's ratio of paste-mortar is 0.2.

(b) The radius of aggregates was taken as unity.

(c) For simplicity α_1 was taken as 1000.

The distance between aggregates d was taken as the variable parameter, i.e. d = 0.05r, 0.1r, 0.2r, etc, or m = 0.025, 0.05, 0.1, etc. This established the stresses as a function of the average distance between aggregates d.

The model stresses for the temporary value $\alpha_1 = 1000$ are:

$$\alpha_x = \alpha_1 + \alpha_{2x} = 1000 + \alpha_{2x}$$

$$\alpha_y = \alpha_1 + \alpha_{2y} = 1000 + \alpha_{2y}$$

$$\tau_{xy} = \tau_{2xy}$$

Results:

The resulting stresses α_x, α_y, τ_{xy} at points O, B, A, 1, 2, 3, C, D obtained from the electronic computer are tabulated in Table 7. The radial, circumferential and corresponding shear stress (α_r, α_c, τ_{rc}) at points 3, C, and D are obtained from α_x, α_y and τ_{xy} by the usual relationship, represented by Mohr's circle, and are also included. From Table 7, Figure 5 to 12 were then plotted for d - 0.05r, 0.14, 0.2r, 0.6r, 0.8r, 1.0r, and 2.0r, respectively. Note that in these figures (a) gives the normal stresses on the boundary OA2C, and (b) the normal stresses on the plane perpendicular to the boundary OA2C. The shearing stresses are zero at all points calculated, except at point 3, where the values were recorded in parenthesis.

The actual stresses in the model is the product of the values given in Table 7 and the constant

$$\frac{1}{1000} \quad \frac{E}{1-\nu} \quad \varepsilon$$

where E: The modulus of elasticity of paste-mortar.

ν: Poisson's ratio of the paste-mortar.

ε: Free shrinkage strain (which, in a concrete, may be due to hydration, moisture and temperature changes, etc.)

Note that τ_{xy} at point 1 should be zero according to Equation (13). Likewise, τ_{xy} should be zero at point 2. This requirement was not taken into account in establishing the simultaneous equations.

The smallness of the numerical values obtained for τ_{xy} at points 1 and 2 represents a check on the accuracy of the calculation of the computer and the point matching method, respectively.

Hand calculation has been carried out to check the process and values obtained by the digiter computer. Take d = 0.4r (i.e. m = 0.2). The coefficients of the nine simultaneous equations are recorded in Table 8. The value in this Table have six digits; however, only five digits are significant. The last digit was thrown in for protection.

Then the nine equations were solved by an electronic computer using the iteration method. The value of the nine unknown is recorded in Table 9. These values have been substituted into the nine equations by hand calculation and shown to be correct.

Finally the stresses at all points were found by substituting the values of A_1 to A_4, B_1 to B_4 into equations (6), (7) and (8). They are recorded in Table10.

In the process of hand calculation (using five significant digits) it was observed that a maximum of four significant digits could be lost due to subtraction of large numbers. Thus, at least one significant digit remains in every value of Table 10. This is confirmed by comparing Table 10 with Table 7 (d = 0.4r). In the calculation of the electronic computer eight significant digits have been used, therefore, at least four significant digits can be obtained. For this reason every digit of the values in Table 7 is significant as far as computation is concerned.

The stresses at point C as a function of the distance between aggregates are plotted in Fig. 13. It is seen that tension at the interface begins to appear when d becomes less than 0.45r. When d = 0.1r the radial bond stress α_r is about one-half of the circumferential mortar stress α_c at point C. Previous research shows that the average ratio of mortar-aggregate tensile bond strength to tensile strength of mortar at 38 days is 0.5, therefore, at this value of d bond cracks begin to occur in preference to cracks through mortar. It must be kept in mind that the ratio mentioned is for 28 days. This ratio decreases with younger concrete was discussed in previous research. Further decrease of d will cause the maximum computed tensile bond stress to increase very rapidly, as shown by the extremely steep tangent of the curve in Fig. 13, being that much more conductive to the development of bond cracks.

The correctness of this stress analysis of the model has been checked by making actual models. Fig. 14 is a photo of an actual model, with four sandstone discs, arranged in a square array, laying on a glass plate coated with mineral oil to prevent fiction. The distance between the discs is approximately 0.4r. Then cement paste was placed between the discs and allowed to dry in air so as to induce a certain shrinkage. The cracking pattern of the paste corresponds beautifully to the stress analysis. Note that three types of cracks occur: (1) Horizontal and vertical

cracks near the shortest distance between discs. (2) The diagonal crack at the largest distance between discs. (3) Bond cracks. The first two kinds of cracks corresponds to the largest tension in the paste (See Fig.8) and the third cracks occur because of the low bond strength between sandstone and paste at young age.

When the distance between aggregates diminishes to d = 0.15r, as shown in Fig. 15, tensile bond stress and therefore bond cracks become predominant. (Note: the bond strength is only a fraction of the paste strength and the ratio of the former to the latter decreases with younger age as shown in previous research.

Discussion:

The above analysis was carried out assuming the cementing substance to shrink. In the case of expansion of the cementing substance it is only necessary to change the sign of all the values in Table 7 and Fig. 5 to Fig. 12. In that case the maximum tensile stress occurs at point 2 of the interface.

It is interesting to first estimate the order of magnitude of tensile bond stress due to drying shrinkage. According to Lea, mortar with proportion 1:3 and w/c ratio of 0.5 has a drying shrinkage $\varepsilon = 0.0012$ after 6 months in air at $70^{o}F$ and 50% R.H. Assuming also $E = 5 \times 10^{6}$psi, $\nu = 0.2$, and the distance between aggregates d = 0.2, the elastic tensile bond at point C set up by this drying shrinkage is:

$$= \frac{244}{1000} \frac{E\varepsilon}{1-\nu} = \frac{244}{1000} \frac{5x10^6}{1-0.2} \ 0.0012 = 1830 \text{ psi}$$

This is five to fifteen times the mortar-aggregate tensile bond strength obtained in previous research at 30 days. Of course the above analysis is somewhat unfair, since two factors, which are neglected in the analysis, will strongly reduce this stress. They are: (1) The aggregates are actually elastic instead of rigid, as assumed in the analysis. (2) Creep of cement gel. However the stress obtained is large enough to be worth considering. This model also shows the mechanism which is operative when concrete disintegrates due to cycles of drying and wetting. Since each cycle results in volume changes, the model explains the tests of Professor Scholer, which show that concrete went to pieces after cycles of drying and wetting.

In the same manner concrete disintegrates due to temperature change, i.e. due to the stresses set up by temperature volume changes in each cycle. This explains the tests of Goldbeck and Meyer.

Since information on volume change during hydration and on tensile bond strength at early ages before the concrete sets are not available, it is difficult to give a conclusive discussion about the effect of volume change during hydration on the existence of bond cracks. However, some reasoning can be offered:

Whether the paste-mortar shrinks or expands during hydration is still controversal. Lea shows that concrete expands during continuous storage in water and he attributes this phenomenon to the hydration of cement. This means that he believes cement paste will expand during hydration. But a recent paper by Del Campo shows that cement paste shrinks during the first 24 hours of hydration. The volume shrinkage at 24 hours is of the order of 1%. Unpublished research at the concrete laboratory of Cornell University, however, has shown that paste (or mortar) expands in the first few hours and then begins to shrink. Under such circumstances it is only logical to discuss both situations - shrinkage and expansion of the paste-mortar.

In the case where paste-mortar shrinks, there are tensile stresses both in the paste-mortar and at the interface. Whether bond cracks or paste-mortar cracks will occur first depends on the relative magnitude of the two ratios. The first of these is the ratio of mortar-aggregate tensile bond strength to tensile strength of mortar, and the second ratio is the ratio of maximum tensile stresses set up at the interface to the maximum stress in the paste-mortar.

No direct information is available about the first ratio at early age before the concrete sets, but a range of variation of this ratio can be derived. The ratio of paste-limestone bond strength to paste strength is about 0.45 at 3 days and 0.82 at

28 days, although the same ratio for sandstone remains at 0.43 for both 3 and 28 days. In any event, an average ratio of paste-aggregate bond strength to paste strength of 0.44 might be used for 3 days. Secondly, the average ratio of paste-aggregate bond strength to paste strength at 28 days is 0.677 (for saw-cut surface) and the average ratio of mortar-aggregate bond strength to mortar strength at 28 days is 0.478. The later is 0.705 of the former because of the effect of sand as discussed in previous research. Therefore the first ratio of mortar-aggregate bond strength to mortar strength at 3 days should be about 0.44 X 0.705 = 0.31. It is further surmised that this ratio will be smaller for even younger age than 3 days. Thus an approximate upper limit for the first ratio is established. On the other hand the lower limit should approach zero before concrete sets, if the hypothesis proposed in previous research that water will accumulate at the interface of aggregate and paste mortar due to electrical charge considerations and rodding of concrete is true. Thus the possible value of the first ratio before the concrete sets (i.e. within 24 hours after pouring) is from 0 to 0.3.

The second ratio is a function of average distance between aggregates d. In a normal concrete mix the average distance between coarse aggregates d varies from 0.1r to 0.3r. In fact, it was calculated as follows: For the most usual concrete with proportion 1:2:4 and w/c ratio of 0.6.

Step 1:

Composition	Relative Weight	Specific Gravity	Relative Volume
Water	0.6	1	0.600
Cement	1	3.15	0.318
Sand	2	2.65	0.753
Gravel	4	2.65	$\frac{1.506}{3.177}$

Percentage volumes of coarse aggregate is $\frac{1.506}{3.177} = 47.3\%$

Step 2: The unit weight of gravel in a compacted state is 96.4 lbs. per cubic feet, while the specific gravity of the gravel is 165.3 lbs. per cubic feet. Thus, the percentage volume of gravel in a compacted state is $\frac{96.4}{165.3} = 58.2\%$

Step 3: The degree of compactness is $\frac{47.3}{58.2} = 81.3\%$

Step 4: $d = 0.14r$

In the same manner the concrete mix which was used in the micro-cracking investigation with proportion of 1:2.91:3.82 and w/c ratio of 0.6 was calculated to have a $d = 0.24r$.

Now, when $d = 0.1r$ the second ratio is 0.45 (See Fig. 11); when $d = 0.2r$ the ratio is 0.28; and when $d = 0.3r$ the ratio is 0.15. Note that these ratios are derived from the two-dimensional plane model. However, it was thought that these ratios should be very close to those existing in the three-dimensional prototype,

because both the tensile stresses at the interface and in the paste-mortar are expected to increase by about the same percentage in the three-dimensional prototype. For example, the tensile stresses at any points of a body due to uniform restrained volume shrinkage is $\frac{E\epsilon}{1-2\nu}$, while the tensile stresses at any points in a plane due to uniform plane shrinkage is $\frac{E\epsilon}{1-\nu}$, so that the tensile stresses in the three-dimensional prototype is $\frac{1-\nu}{1-2\nu}$ times that in the two dimensional model.

Therefore, if the first ratio of mortar-aggregate tensile bond strength to tensile strength of mortar is taken as 0.15, bond cracks will occur in preference to paste-mortar cracks in all concrete.

The observation that very few paste cracks exist in unloaded concrete cylinders is further explained by the consideration that paste-mortar is still in a semi-plastic state during the first 12 hours of hydration. Once the bond cracks occur, the paste-mortar can rearrange itself and release the tensile stress due to volume shrinkage and thus avoid paste cracking.

In the case of volume expansion during hydration the largest tensile stress occurs at point 2, (Fig. 4) of the interface, i.e. at the closest distance between aggregates. Therefore it will definitely produce bond cracks without any possibility of paste-mortar cracks.

POINT	σ_x	σ_y	τ_{xy}	σ_1	σ_c	τ_{max}
			d = 005 r			
0	727	727	0			
B	779	444	0			
A	816	-2372	0			
1	810	-2378	-0007			
2	789	-2398	0320			
3	858	109	638	263	704	311
C	792	792	-220	572	1012	0
D	794	794	-229	565	1023	0
			d = 01 r			
0	612	612	0			
B	719	303	0			
A	750	-1558	0			
1	735	-1570	0063			
2	688	-1603	-0709			
3	873	- 67	4207	74	732	335
C	684	684	- 259	425	943	0
D	678	678	- 233	445	911	0
			d = 02 r			
0	418	418	0			
B	629	190	0			
A	771	- 966	0			
1	750	- 985	0065			
2	669	-1019	-19032			
3	854	- 183	- 70	- 102	772	285
C	560	560	- 316	244	876	0
D	535	535	- 228	307	763	0
			d = 04 r			
0	348	348	0			
B	517	109	0			
A	780	584	0			
1	760	609	0061			
2	613	605	-8383			
3	795	228	- 179	- 204	770	235
C	419	419	- 384	35	803	0
D	380	380	- 213	167	593	0

TABLE 7

POINT	σ_z	σ_x	τ_{xy}	σ_r	σ_θ	$\tau_{r\theta}$
			d = 06r			
0	277	277	0			
B	447	71	0			
A	733	- 421	0			
1	735	- 465	0213			
2	590	- 473	26			
3	738	- 237	- 249	- 271	771	169
C	337	337	- 430	- 93	767	0
D	297	297	- 205	92	502	0
			d = 08r			
0	233	233	0			
B	396	50	0			
A	665	- 323	0			
1	693	- 390	- 0013			
2	590	- 440	53			
3	692	- 247	- 295	- 319	763	123
C	281	281	- 465	- 184	746	0
D	245	245	- 198	47	443	0
			d = 10r			
0	201	201	0			
B	354	36	0			
A	597	- 256	0			
1	646	- 344	0025			
2	598	- 440	71			
3	657	- 260	- 326	- 356	752	93
C	240	240	- 493	- 253	733	0
D	209	209	- 191	18	400	0
			d = 20r			
0	112	112	0			
B	217	7	0			
A	337	- 58	0			
1	465	- 287	- 0086			
2	635	- 497	114			
3	568	- 333	- 397	- 471	727	37
C	129	129	- 574	- 445	703	0
D	113	113	- 148	- 35	261	0

TABLE 7 (CONTINUED)

TABLE 8

EQ	A_1	A_2	A_3	A_4	B_1	B_2	B_3	B_4	Ek	CONST.
(11)	245290	435373	320371	2018.72	139600	108.264	1282 92	11338 2	-120000	0
(12)	.337240	5 32912	25 5247	68 5582	2 31421	18 1887	75 0669	193 840	120000	0
(13)	106508	29 5004	464 005	5285 00	2 66026	122 526	268368	384916	0	0
(14)	2 39959	420538	296 856	1748 25	129778	104 576	1187 61	9819 11	-120000	0
(15)	224012	377045	230 028	1009 36	100239	93 7598	916 837	5669 04	-120000	0
(16)	122415	239157	222 575	1738 84	380382	105 679	1419 65	138921	120000	0
(17)	.504831	780196	33 3208	49 2704	-159696	961408	85 0663	168056	-120000	0
(18)	.751490	123421	64 3986	270 464	260093	410653	306883	1611 77	120000	0
(19)	204408	36 2811	200 970	1082 20	980611	150689	149835	122522	0	-144000

TABLE 9

A_1	15553816
A_2	12995008
A_3	678 61690
A_4	18.182874
B_1	300 04965
B_2	155 47618
B_3	15.584260
B_4	0.58245198
Ek	311.20978

TABLE 10

POINT	σ_x	σ_y	τ_{xy}
0	346	346	
B	520	90	
A	750	- 570	
1	770	- 590	
2	680	- 560	
3	790	- 240	- 170
C	419	419	- 312
D	350	350	

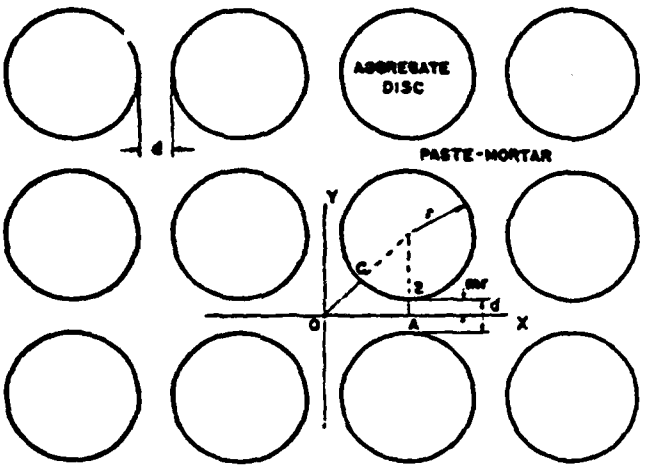

FIG. 3

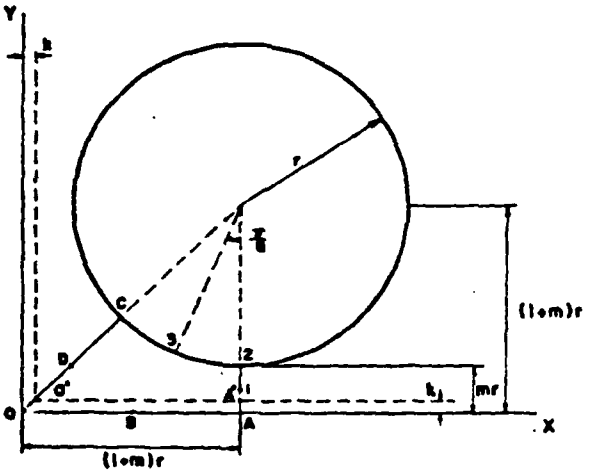

FIG. 4

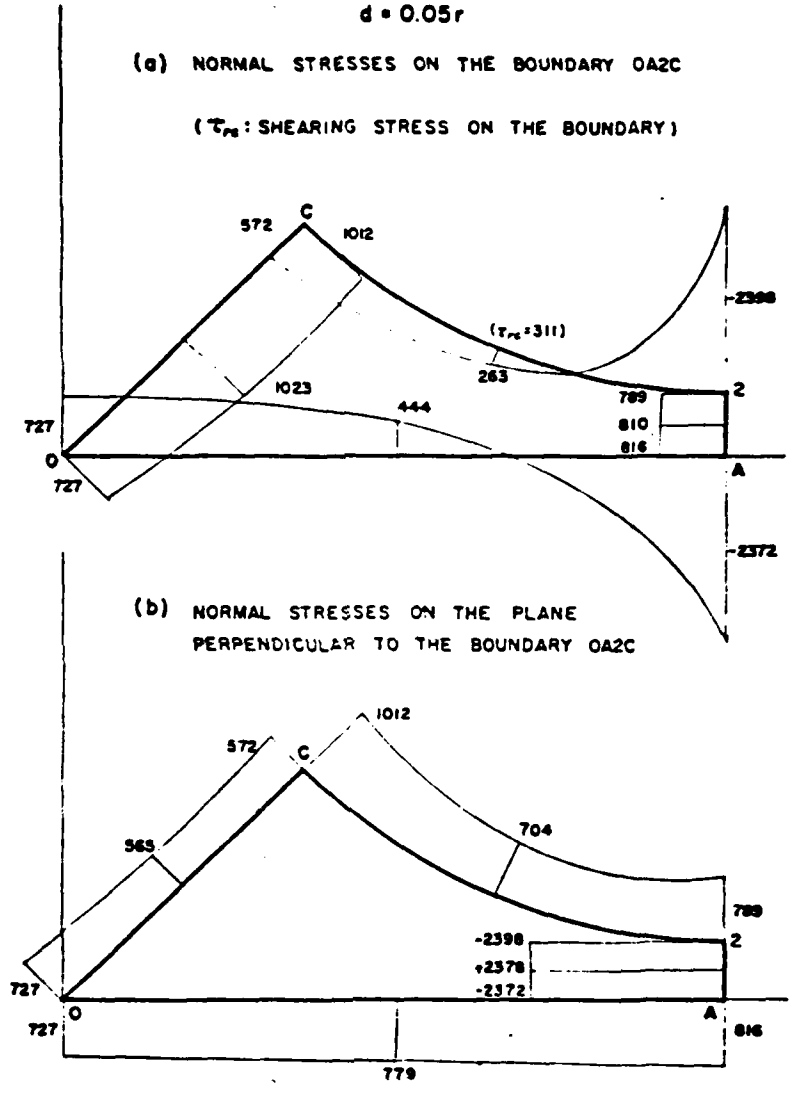
d = 0.05r
(a) NORMAL STRESSES ON THE BOUNDARY OA2C
($\tau_{rθ}$: SHEARING STRESS ON THE BOUNDARY)
572
C
1012
($\tau_{rθ}$=311)
263
1023
444
727
0
727
789
810
816
2
A
-2398
-2372
(b) NORMAL STRESSES ON THE PLANE
PERPENDICULAR TO THE BOUNDARY OA2C
1012
572
C
704
565
789
-2398
+2378
-2372
2
727
0
727
A
816
779

FIG. 5

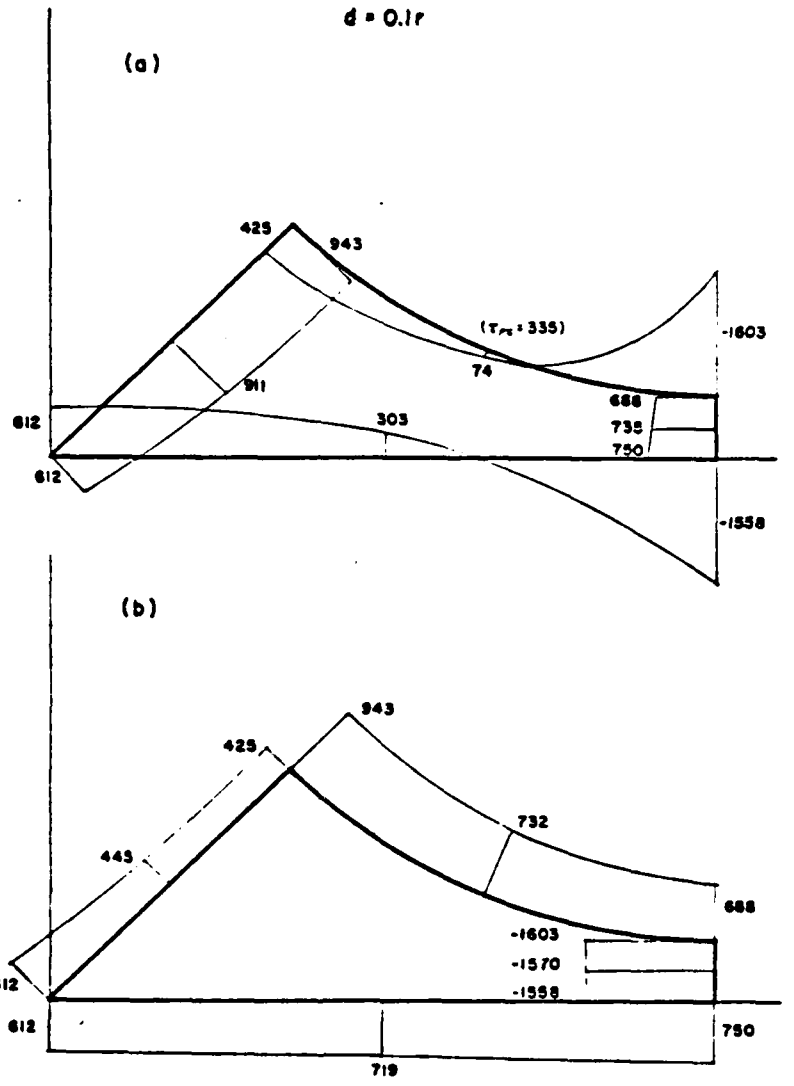
d = 0.1r
(a)
425
943
(T_rc = 335)
-1603
911
74
688
612
303
735
750
612
-1558
(b)
943
425
732
445
688
-1603
-1570
612
-1558
612
750
719

FIG. 6

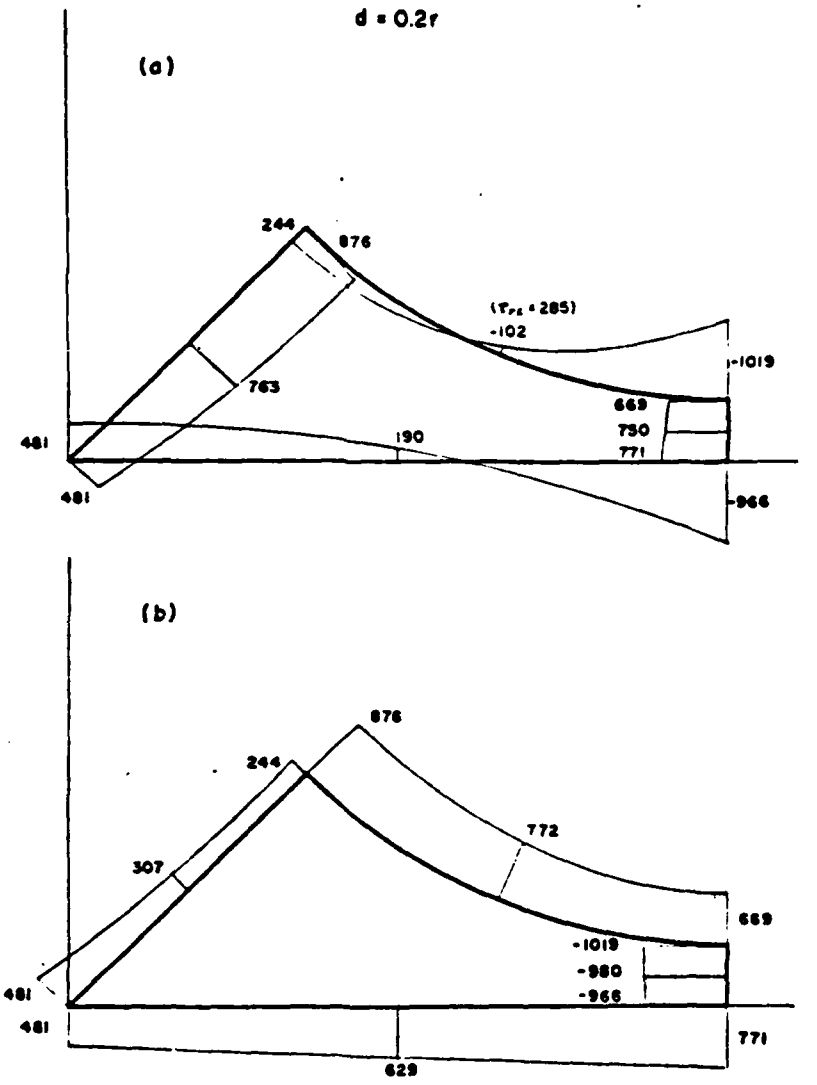
d = 0.2r
(a)
244
876
(T_FS = 285)
-102
-1019
763
669
730
771
481
190
481
-966
(b)
876
244
772
307
669
-1019
-980
-966
481
481
771
629

FIG. 7

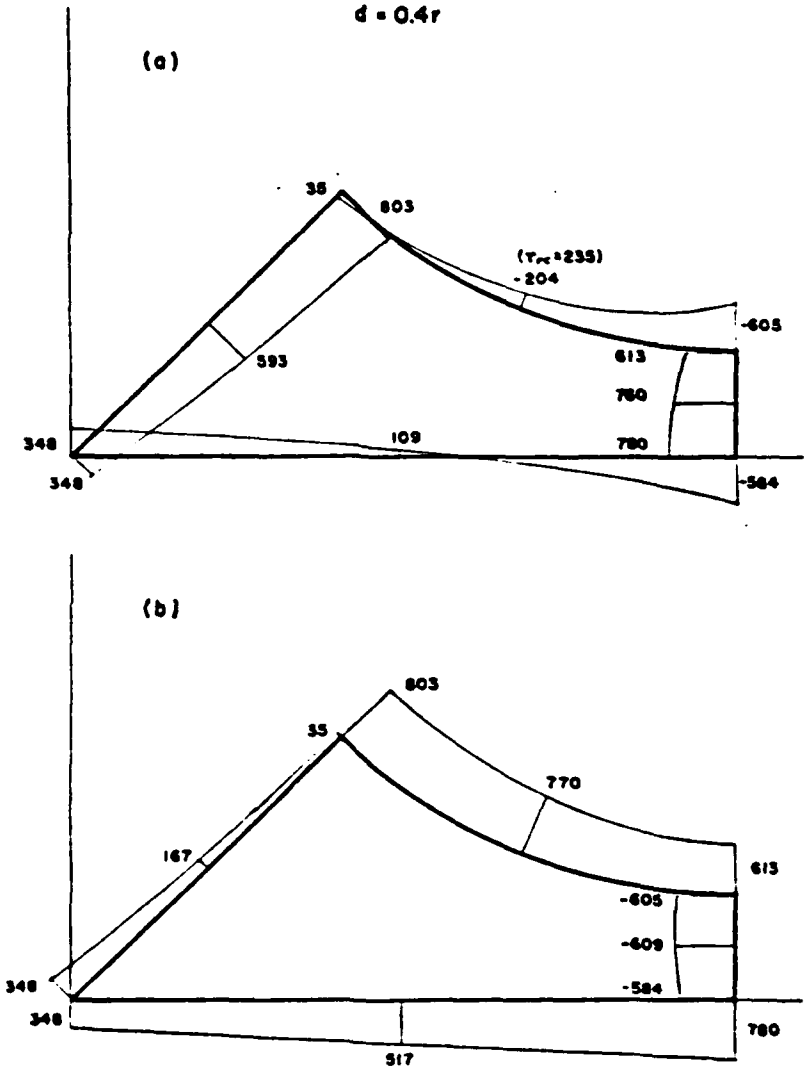
d = 0.4r
(a)
35
803
(T_PC = 235)
-204
-605
593
613
760
348
109
780
348
-584
(b)
803
35
770
167
613
-605
-609
348
-584
348
780
517

FIG. 8

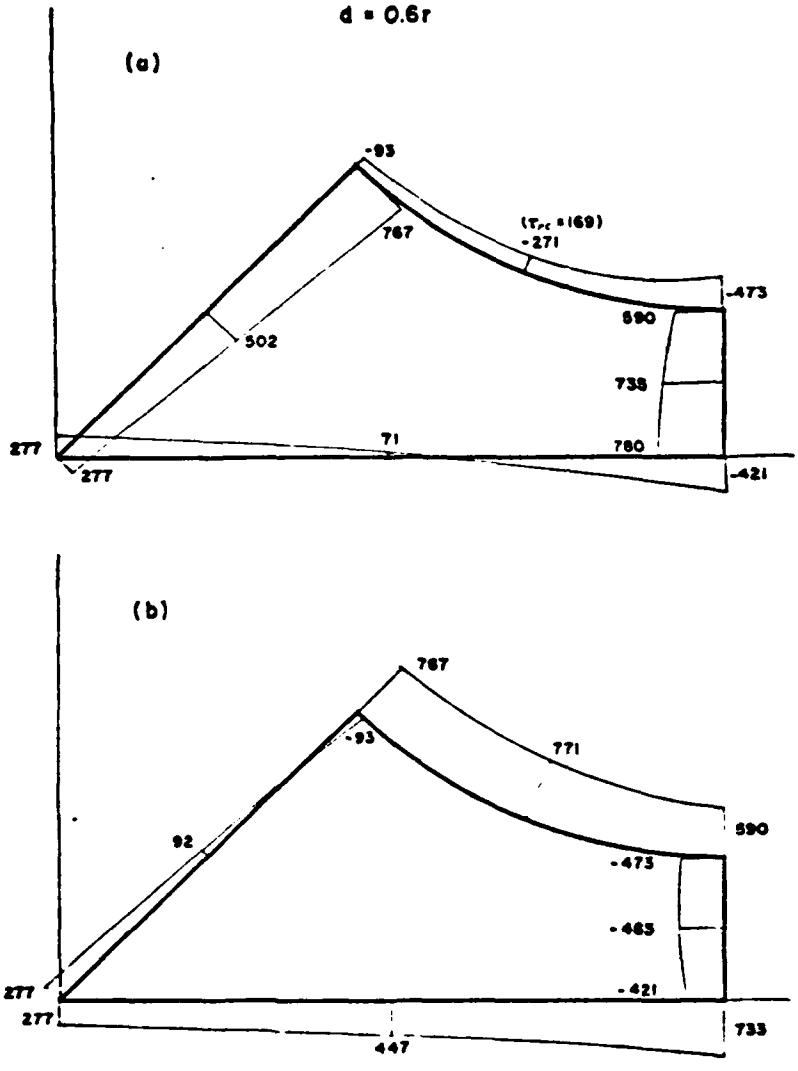
d = 0.6r
(a)
-93
767
(τrc = 169)
-271
-473
590
502
738
71
780
277
277
-421
(b)
767
771
-93
590
92
-473
-465
277
277
-421
733
447

FIG. 9

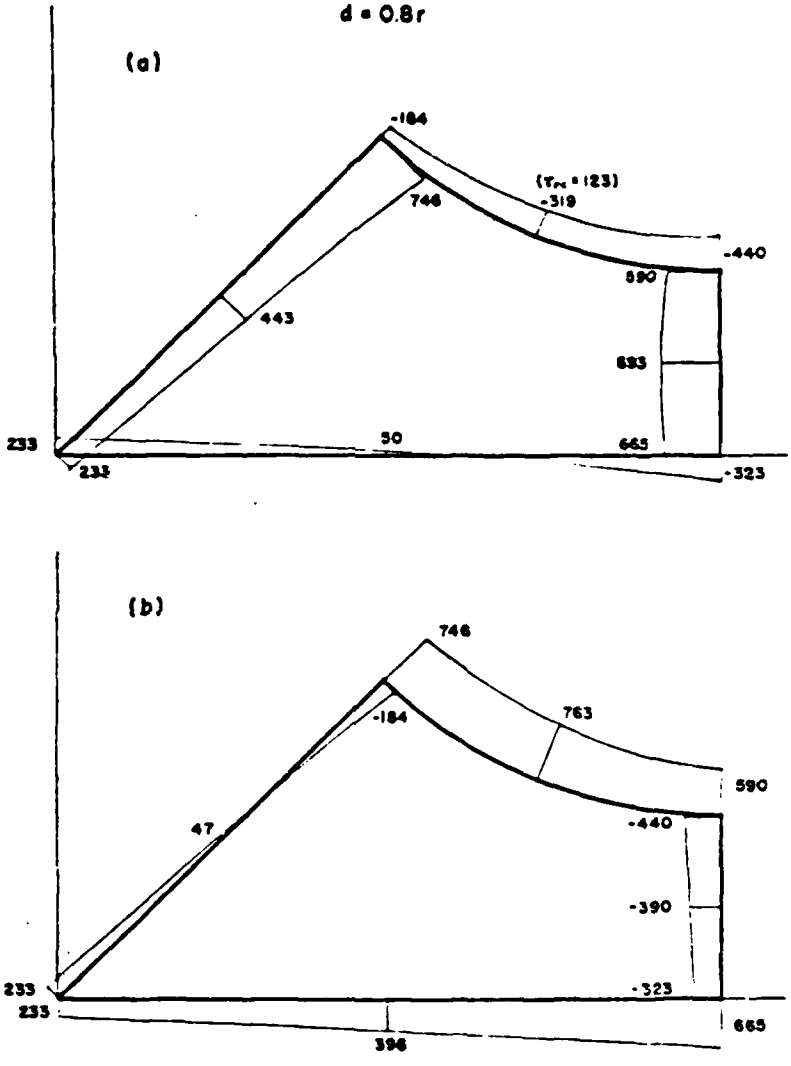
d = 0.8r
(a)
-184
746
(T_H = 123)
-319
-440
890
443
833
233
50
665
233
-323
(b)
746
763
-184
590
47
-440
-390
233
-323
233
665
396

FIG. 10

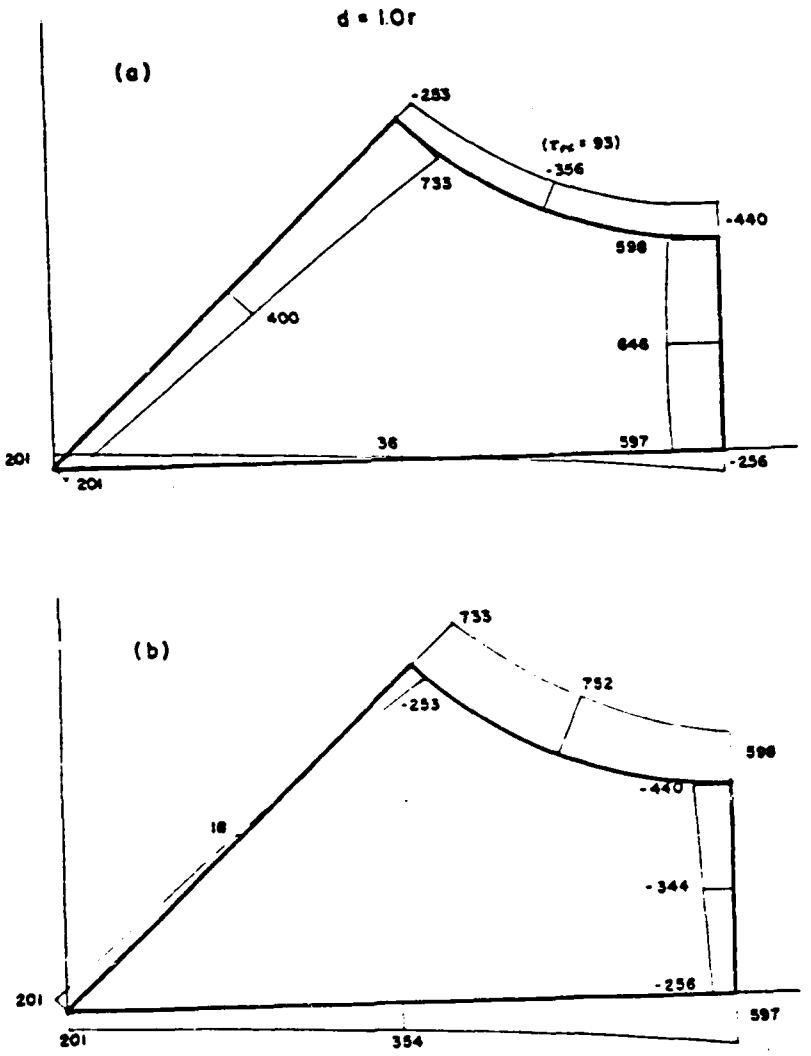
d = 1.0r
(a)
-253
(τ_rz = 93)
-356
733
-440
598
400
646
36
597
201
-256
201
(b)
733
752
-253
598
-440
18
-344
-256
201
597
201
354

FIG. 11

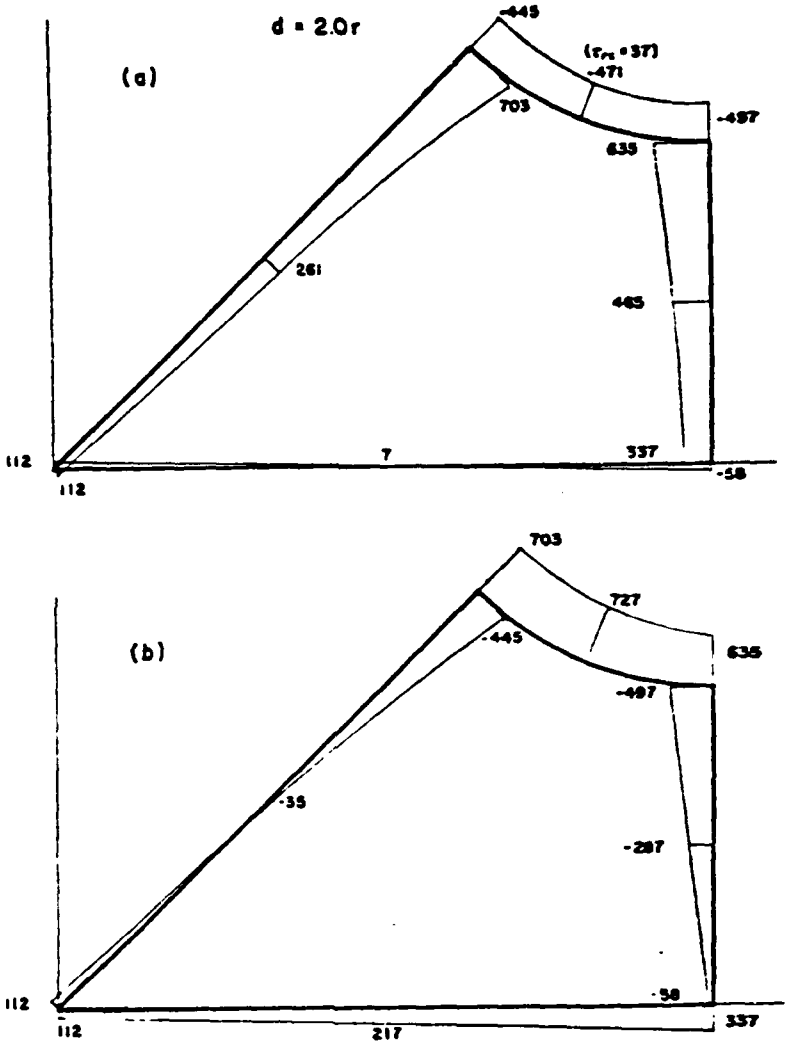
d = 2.0r
(a)
-445
(r_rs = 37)
-471
703
-497
635
261
445
112
7
337
112
-58
(b)
703
727
635
-445
-497
-35
-287
-58
112
112
217
337

FIG. 12

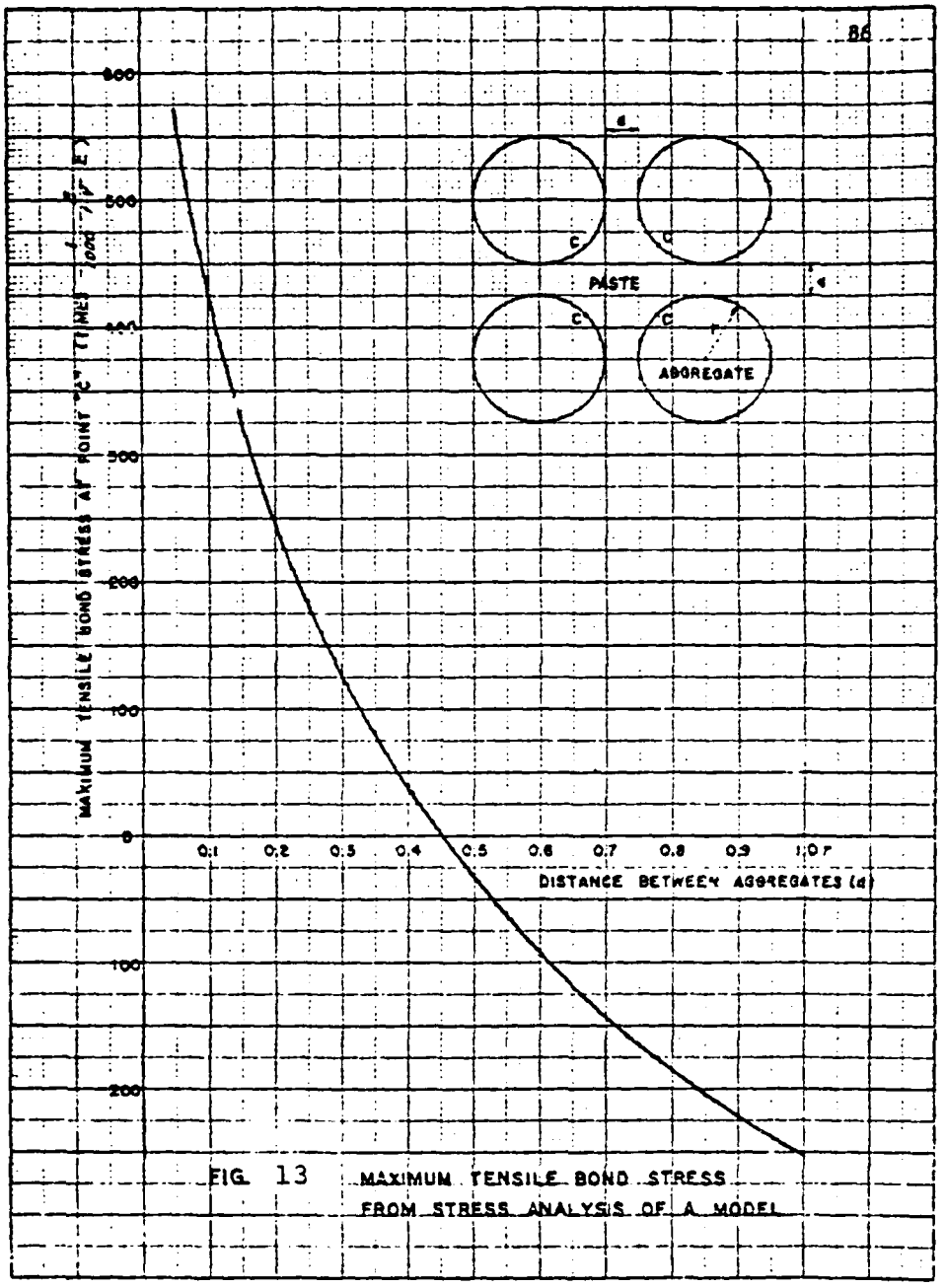

FIG. 13 MAXIMUM TENSILE BOND STRESS FROM STRESS ANALYSIS OF A MODEL

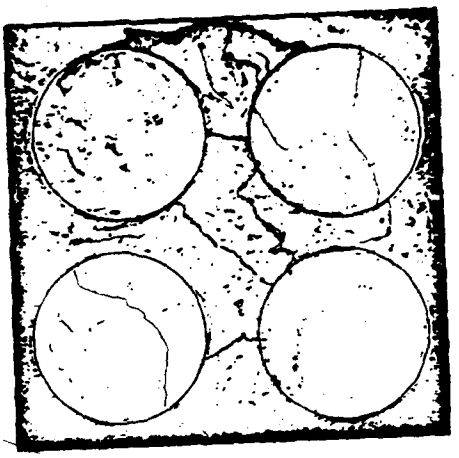

FIG. 14 d = 0.1r

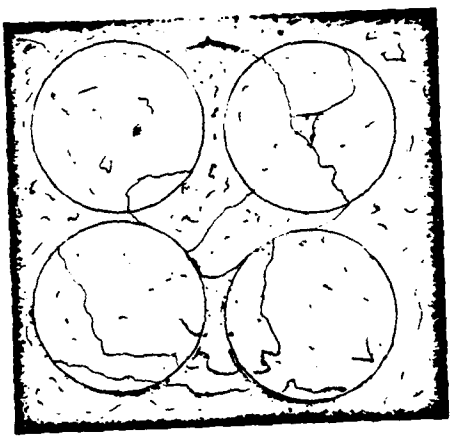

FIG. 15 d = 0.15r

APPENDIX

Following are some photographs taken of the actual micro-cracks which appear in concrete and observed with the Scanning Electron Microscope. The purpose of these photos are to just show a few possibilities which can exist.

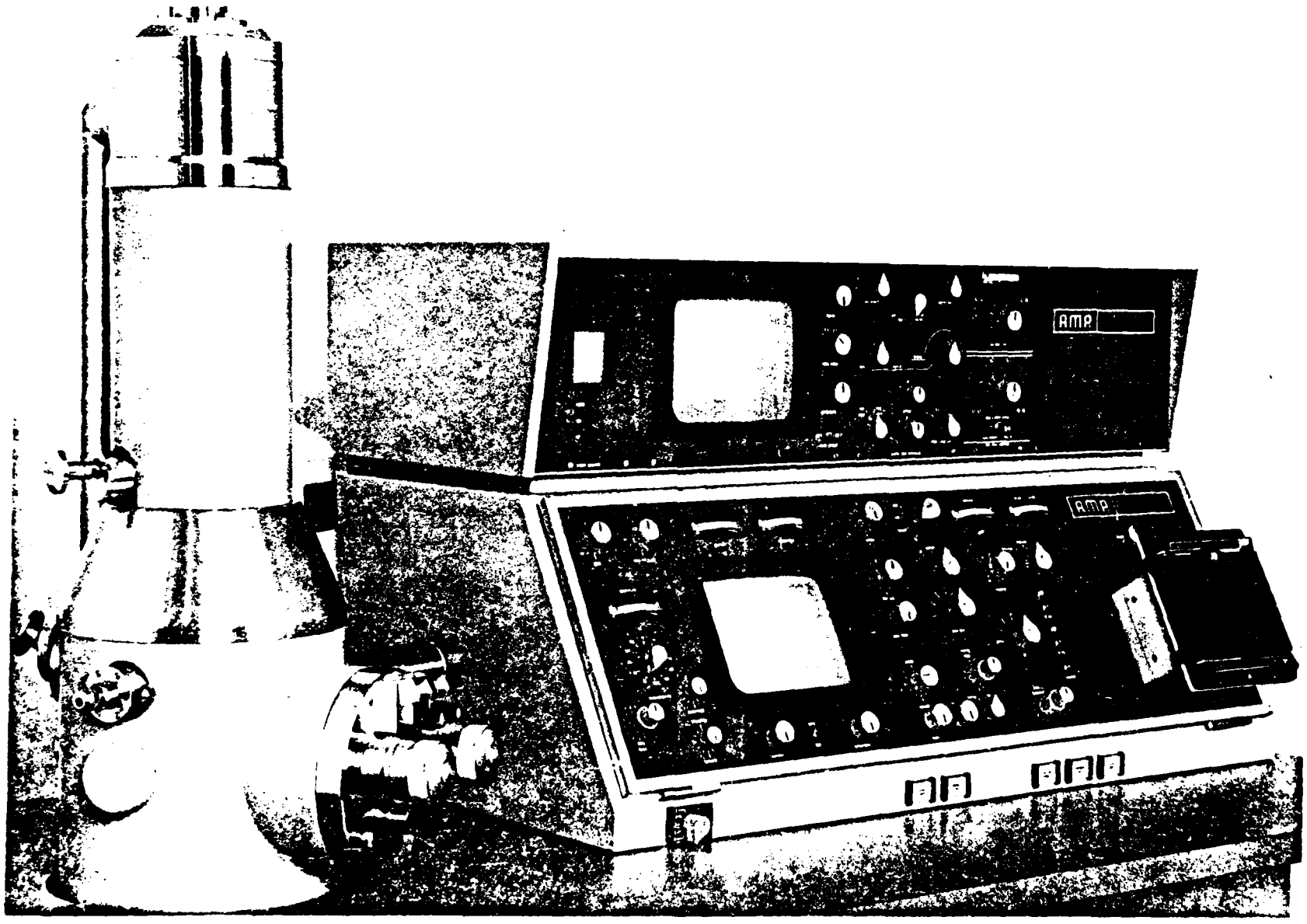

Fig. 1- AMR-1000 SEM

Fig. 2 - Crack map for reinforced limestone concrete (3000 psi) at 0% compression of the ultimate strength (50 x 1.35).

Fig. 3 - Crack map for reinforced aggregate concrete (3000 psi) at 15% biaxial compression of the ultimate strength (100 X 1.50).

Fig. 4 - Crack map for reinforced limestone concrete (3000 psi) at 45% biaxial compression of the ultimate strength (500 X 1.20).

Fig. 5 - Crack map for plain limestone concrete (3000 psi) at 75% biaxial of the ultimate strength (100 X 1.25).

Fig. 6 - Crack map for reinforced aggregate concrete (3000 psi) at 45% axial compression of the ultimate strength (200 X 1.20).

Fig. 7 - Crack map for reinforced limestone concrete (3000 psi) at 75% biaxial compression of the ultimate strength (50 X 1.25).

Fig. 8 - Crack map shows the different cracks between both sides of the reinforcement. R-R-3000 psi at 45% biaxial compression of the ultimate strength (20 X 1.15).

Fig. 9 - Crack map for reinforced limestone concrete (3000 psi) at 15% axial compression of the ultimate strength (5000 X 1.05).

Fig. 10 - Crack map for plain aggregate concrete (3000 psi) at 0% compression (50 X 1.45).

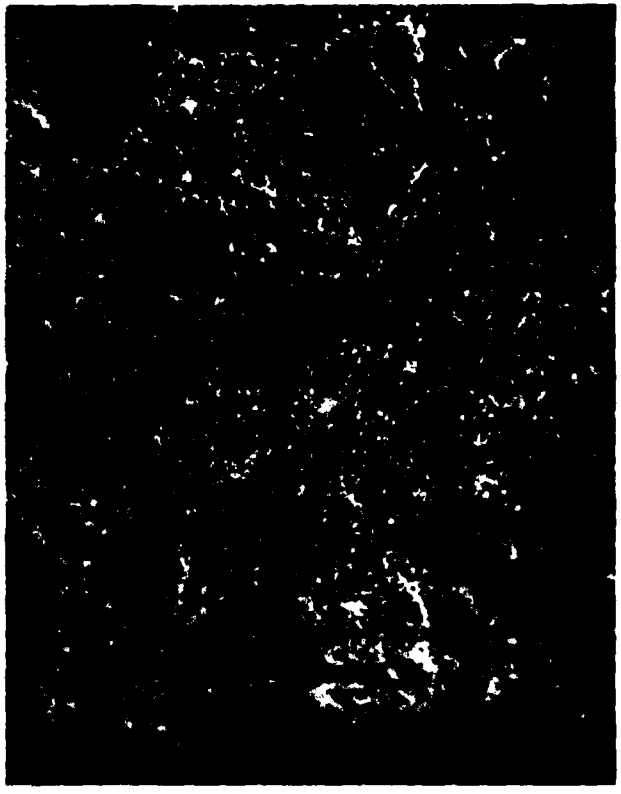

Fig. 11 - Crack map for plain aggregate concrete (4000 psi) at 0% compression shrinkage cracks (200 X 1.35).

Fig. 12 - Crack map for reinforced limestone concrete (4000 psi) at 45% axial compression of the ultimate strength (200 X 1.30).

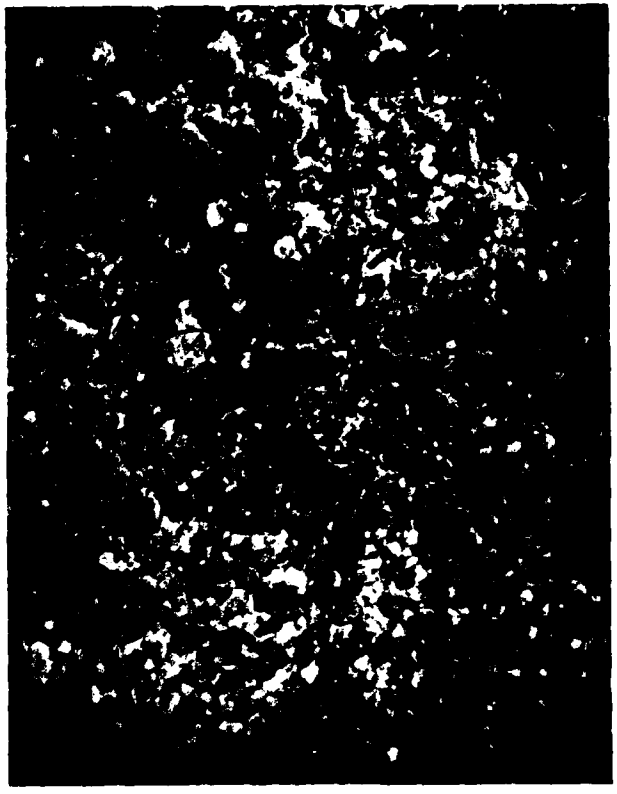

Fig. 13 - Crack map for plain aggregate concrete (4000 psi) at 30% axial compression of the ultimate strength (500 X 1.35).

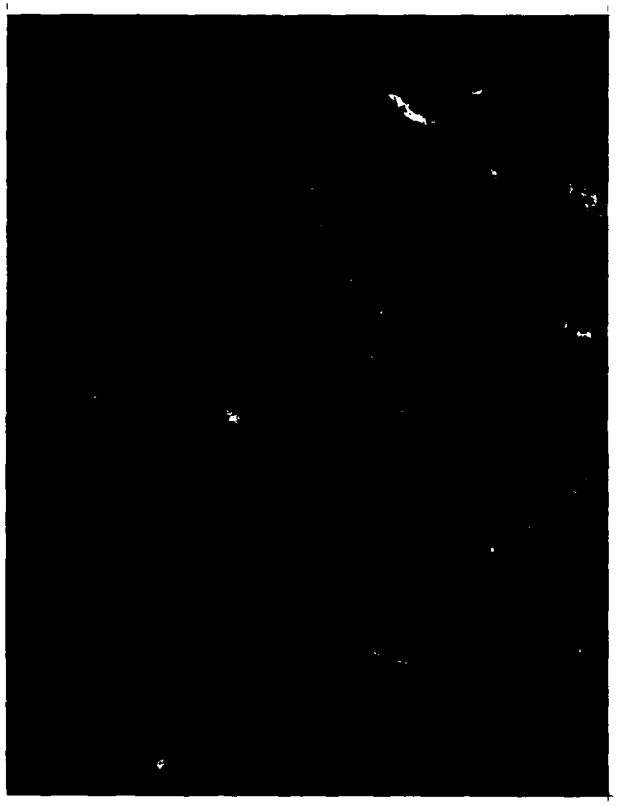

Fig. 14 - Crack map for plain limestone concrete (4000 psi) at 15% biaxial compression of the ultimate strength (50 X 1.35).

Fig.15 - Crack map for plain limestone concrete (4000 psi) at 75% biaxial compression of the ultimate strength (200 X 1.25).

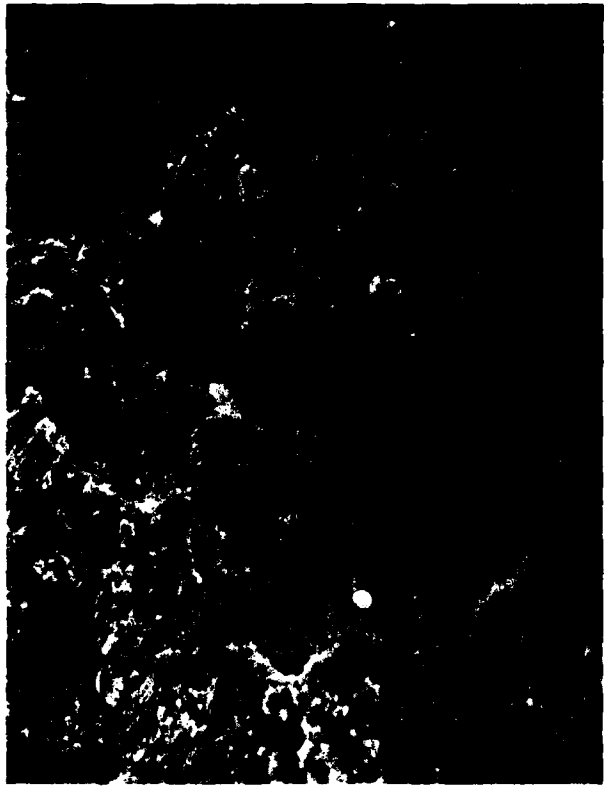

Fig. 16 - Crack map for plain limestone concrete (4000 psi) at 75% biaxial compression of the ultimate strength (2000X 1.35).

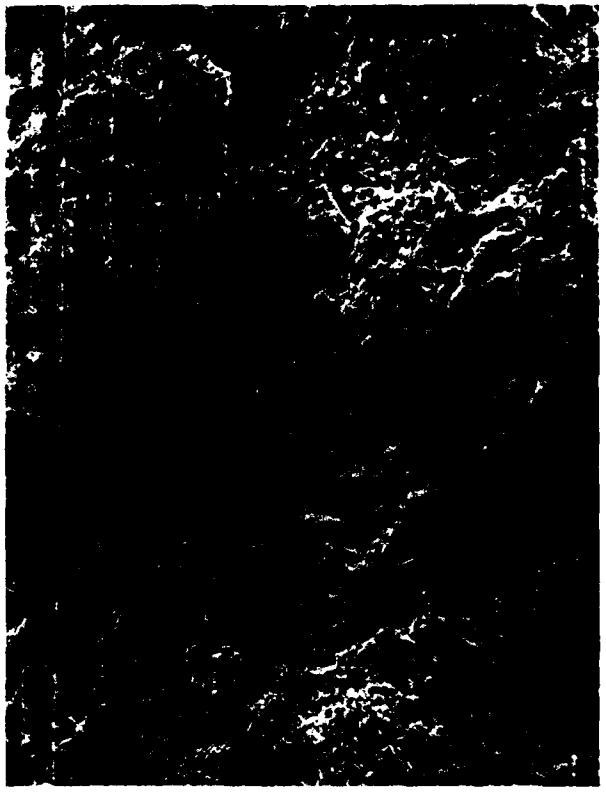

Fig. 17 - Crack map for reinforced aggregate concrete (4000 psi) at 65% biaxial compression of the ultimate strength (50 X 1.45).

AD-A141 788 APPLICATIONS OF THE SCANNING ELECTRON MICROSCOPE TO CONCRETE FAILURE (AXI..(U) STEVENS INST OF TECH HOBOKEN N J K DERUCHER 05 MAR 84 AFOSR-TR-84-0431 2/2

UNCLASSIFIED AFOSR-80-0256 F/G 11/2 NL

END
DATE FILMED
7 84
DTIC

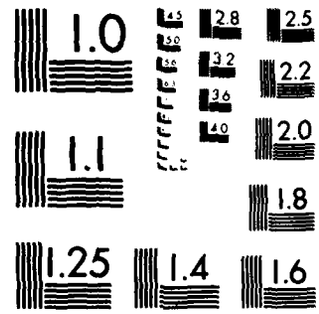

Fig. 18 - Crack map for plain aggregate concrete (4000 psi) at 0% compression (50 X 1.30)

Fig. 19 - Crack map for reinforced aggregate concrete (4000 psi) at 45% biaxial compression of the ultimate strength (200 X 1.45).

Fig. 20 - Crack map for plain limestone concrete (5000 psi) at 45% axial compression of the ultimate strength (200 X 1.50).

Fig. 21 - Crack map for plain limestone concrete (5000 psi) at 45% axial compression of the ultimate strength (50 X 1.50).

Fig. 22 - Crack map for reinforced limestone concrete (5000 psi) at 45% axial compression of the ultimate strength. Cracks along the reinforcement (2000X 1.40).

Fig. 23 - Crack map for reinforced limestone concrete (5000 Psi) at 0% compression. Shrinkage cracks (5000X 1.40).

REFERENCES

General:

1. A. Brandtzaeg, Study of the failure of concrete under combined stresses. UIEES Bull. 185 (1928).

2. O. Berg, The factors controlling concere strength. Construc. Rev. 33 (11), 19 (1950).

3. R. Jones, A method of studying the formation of cracks in a material subjected to stress. Br. J. Appl. Phys. 3, 229 (1952).

4. J. L'Hermite, Present day ideas on concrete technology - 3. The failure of concrete, union of testing and research laboratories for materials and structures. Bull. 18, 27-39 (1954).

5. E. Hognestad, Concrete stress distribution in ultimate strength design. J. Amer. Concrete Inst. 27(4) (1955).

6. H. Rusch, Physical problems in the testing of concrete, Cement-Chalk 12(1), 1-9 (1959).

7. J. Robinson, X-ray analysis of concrete fracture. J. Am. Concrete Inst. 50(8) (1959).

8. T. Hsu, F. Slate, G. Sturman, and G. Winter, Microcracking of plain concrete and the shape of the stress-strain curve. J. Am. Concrete Inst. 60(2), 209-224 (1963).

9. T.C. Hansen, Microcracking of concrete. J. Am. Concrete Inst. 64(2), 9-12, (1968).

10. G. Sturman, Shrinkage microcracks in concrete. Ph.D. Dissertation, Cornell University (1969).

Specific:

1. M. Del Campo, A New Method to Study the Early Volume Changes on the Neat Cement Paste, RILEM Bull. 4 Oct. 1959.

2. A.T. Goldbeck, Research Needed on Accelerating Weathering Tests, the Crushed Stone Journal, pp. 8-12 Sept-Oct. 1939.

3. F.A. Lea, The Chemistry of Cement and Concrete, Edward Arnold (Publishers) Ltd., 1956.

4. S.L. Meyers, How Temperature and Moisture Changes May Affect the Durability of Concrete, Rock Product, Vol. 54(8), 1951.

5. C.H. Scholer, A Wetting and Drying Test for Predicting Cement Aggregate Reaction, Kansas State College Bulletin XXXIV, 1950.